Atmos. Chem. Phys. Discuss., 11, 26245–26345, 2011
www.atmos-chem-phys-discuss.net/11/26245/2011/
doi:10.5194/acpd-11-26245-2011

Atmospheric Chemistry and Physics Discussions

ExchanGE processes in mountainous Regions (EGER) – overview of design, methods, and first results

T. Foken[1,g], F. X. Meixner[2,4], E. Falge[2], C. Zetzsch[3,g], A. Serafimovich[1,g], A. Bargsten[2], T. Behrendt[2], T. Biermann[1], C. Breuninger[2], S. Dix[1,a], T. Gerken[1], M. Hunner[1,a], L. Lehmann-Pape[2], K. Hens[2], G. Jocher[1,b], J. Kesselmeier[2], J. Lüers[1,g], J.-C. Mayer[2], A. Moravek[2], D. Plake[2], M. Riederer[1], F. Rütz[1], M. Scheibe[2,c], L. Siebicke[1,d], M. Sörgel[3], K. Staudt[1,e], I. Trebs[2], A. Tsokankunku[2], M. Welling[2], V. Wolff[2,e], and Z. Zhu[2,f]

[1]University of Bayreuth, Department of Micrometeorology, 95440 Bayreuth, Germany
[2]Max-Planck-Institute of Chemistry, Biogeochemistry Department, P.O. Box 3060, 55020 Mainz, Germany
[3]University of Bayreuth, Atmospheric Chemistry Research Laboratory, 95440 Bayreuth, Germany
[4]University of Zimbabwe, Department of Physics, P.O. Box MP 167, Mount Pleasant, Harare, Zimbabwe

[a]now at: TÜV Süd Industrie Service GmbH Wind Cert Services, Ludwig-Eckert-Straße 10, 93049 Regensburg, Germany
[b]now at: Alfred-Wegener Institute for Polar and Marine Research, Telegrafenberg A43, 14473 Potsdam, Germany
[c]now at: German Aerospace Center (DLR), Institute of Atmospheric Physics, Münchner Straße 20, 82234 Oberpfaffenhofen-Wessling, Germany
[d]now at: Institut national de la recherche agronomique (INRA), BP 709, 97387 Cedex Kourou, French Guiana
[e]now at: Agroscope ART Research Station, Reckenholzstrasse 191, 8046 Zürich, Switzerland
[f]now at: Institute for Geographic Sciences and Natural Resources Research, ChineseAcademy of Sciences (CAS), A11 Datun Road, Anwai, Beijing 100101, China
[g]Member of Bayreuth Center of Ecology and Environmental Research (BayCEER), University of Bayreuth, 95440 Bayreuth, Germany

Received: 10 July 2011 – Accepted: 6 September 2011 – Published: 21 September 2011

Correspondence to: T. Foken (thomas.foken@uni-bayreuth.de)

Published by Copernicus Publications on behalf of the European Geosciences Union.

Abstract

To investigate the energy, matter and reactive and non-reactive trace gas exchange between the atmosphere and a spruce forest in the German mountain region, two intensive measuring periods were conducted at the FLUXNET site *Waldstein-Weidenbrunnen* in September/October 2007 and June/July 2008. They were part of the project "ExchanGE processes in mountainous Regions" (EGER). Beyond a brief description of the experiment and links to the already published results of both experiments, the main focus of the paper is the problem of the coupling of the trunk space, the canopy and the atmosphere. Therefore, the relevant coherent structures were analyzed in different canopy levels and an already published coupling classification was applied to gradients and fluxes. It could be shown that fluxes above the canopy are only related to the gradient between the canopy and the atmosphere in the case of a fully coupled system. Changes in the concentration of especially reactive trace gases (NO-NO_2-O_3 and HONO) could only be interpreted together with the coupling stage. Finally it was pointed out that the combination of air chemical measurements with micrometeorological turbulence measurements is urgently needed to understand the biosphere-atmosphere interaction.

1 Introduction

The scientific focus on forest ecosystems has long been the privilege of more than the ecologist. The forest is also a real challenge for micrometeorologists and atmospheric chemists. In the book by Hutchinson and Hicks (1985) the very complex character of the exchange processes between the atmosphere and the forest was highlighted and some of the specific problems like counter-gradients and their consequences were made public for a larger community (Denmead and Bradley, 1985). Other issues like the roughness sublayer (Garratt, 1978, 1980) were taken into account. For a better understanding of the forest atmosphere interaction the mixing layer

hypothesis became an important contribution (Finnigan, 2000; Raupach et al., 1996) and recently a common theory for the roughness sublayer and mixing layer has seemed to be possible (Harman and Finnigan, 2007, 2008). The approach of the mixing layer theory is closely connected with coherent structures (Collineau and Brunet, 1993a, b; Katul et al., 1997) which generate typical ramp structures in the time series of scalar quantities measured above a forest. Such ramp structures could also be found in trace gas fluctuations (Rummel et al., 2002). While for the measurement of turbulent fluxes of momentum, sensible heat, water vapour and carbon dioxide the fast response and direct eddy-covariance technique is state-of-the-art, slow response flux measuring techniques had be applied for most trace gases and aerosol particles, like the aerodynamic method (Arya, 2001; Monteith and Unsworth, 2008) or the modified Bowen-ratio method (Businger, 1986). During the last decade, however, the eddy-covariance technique has become applicable for aerosol particles and a selected number of trace gases – particularly, nitrous oxide (N_2O), methane (CH_4), ozone (O_3), nitric oxide (NO) and nitrogen dioxide (NO_2) (e.g. Rummel et al., 2002; Güsten and Heinrich, 1996; Horii et al., 2004; Pryor et al., 2007; Griffith et al., 2002).

Concepts of micrometeorological measurements, focusing on the exchange of energy and carbon dioxide in and above tall vegetation, have already been formulated in such a way that related phenomena like advection (Aubinet et al., 2003; Lee, 1998), roughness sublayer and mixing layers (Finnigan, 2000; Raupach et al., 1996), as well as coherent structures (Collineau and Brunet, 1993a, b) could be detected. However, better understanding of turbulence structures in and above forest canopies require the investigation of coherent structures in greater detail. Furthermore, as shown by Raupach (1981) and Bergström and Högström (1989), coherent events of low frequency contribute significantly to the budgets of momentum, heat and trace substances in and above forest canopies.

While the eddy-covariance flux measuring technique is relevant and state-of-the-art for intensive investigations of fluxes of energy and trace substances in and above forest canopies, the corresponding flux methodology still needs better understanding

(Aubinet et al., 2000; Moncrieff et al., 1997). It soon became obvious that the concept of a flux through an interface had to be replaced by a flux through a volume element; consequently, (3-D) advection became a substantial problem (Aubinet et al., 2003; Lee, 1998; Paw U et al., 2000). Though this problem could not be solved satisfactorily (Aubinet, 2008; Aubinet et al., 2010), advection-related field experiments performed to date have supported our understanding of forest ecosystems.

Forest canopies as well as forest soils absorb and/or emit carbon dioxide, water vapour and a variety of non-reactive and reactive trace substances (e.g. SO_2, N_2O, CH_4, VOC, O_3, NO, NO_2, HONO, HNO_3, NH_3), and corresponding aerosol compounds (SO_4^{2-},NH_4^+, NO_2^-, NO_3^-). Canopy uptake of air pollutants (SO_2, O_3, NO, NO_2, NH_3, NH_4^+) and acidic compounds (H_2SO_4, HONO, HNO_3, SO_4^{2-}, NO_3^-) is a known and long-standing issue of air pollution control and forest dieback. However, the ability of forest canopies to absorb trace gases, which are biogenically emitted by plants and/or by the soil below, became recently known to be an important aspect of atmospheric budgets of trace substances (cf. Ganzeveld et al., 2002). In the case of soil CO_2 respiration and soil biogenic NO emission, considerable amounts of these trace gases can be (re-)absorbed by understory and/or forest canopy vegetation before they can escape the forest into atmospheric surface and boundary layers, and finally into the free troposphere (Vogel, 1978). Generally, the amount of absorbed/escaping trace gases is controlled (a) by physiological and/or surface characteristics of forest vegetation and soils, and (b) by the interaction of turbulent transport (in and above canopy) with processes of the gas exchange itself and atmospheric transformations of chemically reactive trace compounds. The latter issue can be focused on the question of coupling, namely how strongly is the entire forest atmosphere (or parts of it) coupled to (or de-coupled from) the surface layer above the canopy. This has substantial consequences for the mean residence time (hence, the in-canopy recycling) of trace compounds (cf. Aubinet et al., 2003; Meixner et al., 2003). Low coupling (de-coupled) situations, resulting in longer residence times, generally favor the efficiency of reactions and transformations between chemically reactive trace gases (e.g. triads of NO-NO_2-O_3 and HNO_3-NH_3-

$NH_4NO_{3,aerosol}$). For example, once NO is emitted from the forest soil, it is oxidized by O_3 (imported from aloft) to NO_2, which may undergo reverse photo-dissociation. Characteristic time scales of both reactions are in the order of minutes and might be in the same order as, or even faster than, characteristic time scales for in-canopy transport (cf. Gut et al., 2002). Consequently, 100 % of the soil biogenic NO can easily be converted to NO_2 close to the forest floor, since shading reduces photolysis of NO_2 there (Meixner et al., 2003). To a certain extent, the generated NO_2 is deposited to soil and vegetation surfaces over the whole depth of the canopy and only a fraction of the soil emitted NO (in form of NO_2) will escape to the surface layer above the canopy.

For the investigation of in-canopy storage, canopy cycling, and whole ecosystem exchange of reactive trace gases, measurements of vertical profiles of concentrations and fluxes are essential. While methodologies to measure vertical concentration profiles for NO, NO_2, O_3, NH_3, HONO, HNO_3 (NH_4^+, NO_3^-) are state-of-the-art (cf. Trebs et al., 2004), flux measurements of these compounds by the eddy covariance technique have been (and still are) hampered by the unavailability of fast and specific chemical sensors. However, Rummel et al. (2002) have demonstrated operational eddy covariance flux measurements of NO by applying a specific and fast chemiluminescence analyzers. Horii et al. (2004) applied operational eddy covariance flux measurements of NO and NO_x over a temperate deciduous forest, and recently Farmer et al. (2006) presented a thermal-dissociation laser-induced fluorescence method to perform fast (EC) measurements for fluxes of HNO_3, Σalkyl nitrates, Σperoxy nitrates, and NO_2.

Against this background the authors joined forces to study diel cycles of energy, water, non-reactive and reactive trace compounds in the soil–vegetation–boundary layer-system. In the frame of the project “ExchanGE processes in mountainous Regions (EGER)” joint field experiments focusing on the micrometeorology and the behaviour of trace compounds of a spruce-forest site have been performed at the FLUXNET site DE-Bay (*Waldstein-Weidenbrunnen*) in the *Fichtelgebirge* mountains (Germany).

From the micrometeorological perspective, primary focus of our field studies was the contribution of coherent structures to the transfer of energy, carbon dioxide,

water vapour, and trace compounds at the *Waldstein-Weidenbrunnen* site. Our previous investigations on atmosphere-forest ecosystem coupling at the *Waldstein-Weidenbrunnen* site have been based on the mixing layer theory (Finnigan, 2000; Raupach et al., 1996). Our first approach defined coupling in relation to characteristic length scales of the distance between coherent eddies and the wind shearing (Wichura et al., 2004; Wichura, 2009). Later, a wavelet transform based technique (Thomas and Foken, 2005, 2007b) has been used, which had been developed for the WALDATEM-2003 experiment (Thomas and Foken, 2005, 2007b). There, the mean temporal scales of coherent structures were estimated via the fitting of a normal Gaussian distribution function to the probability density function of the results from the individual 30-min intervals. In 2003, Thomas et al. (2006) extended our research at the *Waldstein-Weidenbrunnen* site by the first investigation of the boundary layer structure over the forest with particular emphasis on coherent structures.

The rationale for both the experimental and modelling design of the EGER studies was based on the analysis of the spatial and temporal scales of the relevant exchange processes in the forest atmosphere, plants and soil (see Sect. 2.4.1 for details). As a first consequence, we limited the overall spatial scale of our experiment to some 100 m × 100 m ("stand/plot scale"). The constraint on the temporal scales to be considered originates from the Damköhler number (Damköhler, 1940), a ratio of two particular time scales, namely the characteristic turbulent transport time over the characteristic chemical reaction time. A Damköhler number (*DA*) less than unity indicates that turbulent transport is faster than chemical reaction; for $DA \leq 0.1$ reactive trace compounds are considered to be treated as (quasi-)passive scalars.

While characteristic chemical reaction times simply result from ambient concentrations, reaction kinetics, (photo-) chemical constants (NO-NO_2-O_3), and thermodynamic equilibrium considerations (NH_3-HNO_3-NH_4NO_3), determination of the corresponding spatial scale is more difficult. The characteristic turbulent transport time is a measure of the intensity of turbulent transport. In the surface layer and under near neutral conditions (cf. Wyngaard, 1982), it may be defined by roughness

length, height above ground, and the ratio of the vertical velocity variance and the friction velocity (Vilà-Guerau de Arellano, 2003). Mayer et al. (2011) present an alternative, stability-dependent definition of the turbulent transport, based on the gradient approach. The questions of both definition and determination of characteristic transport time scales (i.e. available volumes for chemical reactions) within the forest canopy remain open; here, we attempt to tackle the problem through investigation of coherent structures and their effect on coupling of different layers within the canopy with the surface layer above the canopy.

Concentrations of a variety of trace substances can only be measured by slow-response analyzers, like the compounds of the NH_3-HNO_3-NH_4NO_3 triad (Trebs et al., 2004). Consequently, application of all kinds of gradient approaches (e.g. aerodynamic gradient method) is necessary to determine corresponding vertical turbulent fluxes (cf. Thomas et al., 2009). However, over (aerodynamically rough) forest vegetation, the application of these methods is constrained to heights of about twice the canopy height, because below this height the similarity laws may be considerably disturbed due to enhanced surface roughness of the forest. This layer is the so-called roughness sublayer (Garratt, 1978, 1980; Raupach and Legg, 1984; Raupach et al., 1980). In this layer weaker vertical gradients were found, but the turbulent transport is very effective due to coherent structures in the mixed layer (Finnigan, 2000; Raupach et al., 1996). To account for the impact of enhanced roughness, flux-gradient formulations are extended by including a further function, the so-called enhancement factor (Raupach and Legg, 1984; Simpson et al., 1998); explicit functions were given by Garratt (1992) and by Cellier and Brunet (1992). Recently, Harman and Finnigan (2007, 2008) presented a more sophisticated method to consider coherent structures in the mixing layer for the determination of momentum and scalar fluxes, featuring dependence on the mixing layer length scale. In our study, particular emphasis in this direction is given to the application of the aerodynamic method to vertical gradients of the NH_3-HNO_3-NH_4NO_3 triad. As already mentioned above, turbulent fluxes of carbon dioxide, water vapour and the NO-NO_2-O_3 triad have been measured by the

eddy covariance technique, accompanied by careful analysis of all radiation and energy fluxes. To investigate horizontal in-canopy structures (advection), special setups of carbon dioxide measurements have been designed.

In order to elucidate formation pathways of nitrous acid (HONO), an important precursor of OH radicals in the lower troposphere, we included in- and above canopy measurements of HONO mixing ratio in our study. There is agreement that in the absence of light the heterogeneous HONO formation (net reaction: $2NO_2 + H_2O \rightarrow HONO + HNO_3$) is the most important formation pathway, but the mechanisms have not yet been clarified. The reduction of NO_2 by organic species might also be important under atmospheric conditions (Ammann et al., 2005; Gutzwiller et al., 2002). During daytime the main HONO sink is the photolysis $HONO + h\upsilon \rightarrow NO + OH$. However, recent measurements showed that gas-phase formation and the parameterized dark formation are too slow to explain measured HONO concentrations during daytime, which are significantly higher than those calculated from the photostationary state (Kleffmann et al., 2005). An additional daytime source was postulated and described by a recent overview (Kleffmann, 2007). The forest canopy provides a large surface for heterogeneous reactions as well as shading of below canopy space, resulting in different source and sink strengths above and below canopy. These differences, mirrored in concentration differences, were analysed with respect to the coupling of the forest and the air layer above the forest by coherent structures.

In-canopy models FLAME (Berger et al., 2004; Inclan et al., 1996) and CACHE (Stockwell and Forkel, 2002; Forkel et al., 2006) have already been tested at the *Waldstein-Weidenbrunnen* site. Here, the modelling concept involves a 3-D model with a nested structure (STANDFLUX, Falge et al., 1997, 2000) and a 1-D canopy-surface layer model (ACASA, Pyles et al., 2000). The application of a higher order closure model like ACASA is necessary to overcome the counter-gradient problem and also to model the probable influence of coherent structures.

We will present an overview of the EGER project, its design, the applied methods, and particularly of first results from both Intensive Observation Periods, namely

September/October 2007 (IOP-1) and June/July 2008 (IOP-2). Concerning the latter, we focussed our analysis on the coupling between the (above canopy) surface layer, the canopy and the sub-canopy and its consequences for (a) the structure of the turbulent exchange, (b) above canopy fluxes, as well as (c) concentration gradients of non-reactive and reactive trace gases between the surface layer and the forest floor.

2 Material and methods

2.1 Site description

As the research area for this study the *Waldstein-Weidenbrunnen* site (50°08′31″ N, 11°52′01″, 775 m a.s.l.) in the *Fichtelgebirge Mountains* (Germany) was selected. It is located in the Lehstenbach catchment in NE Bavaria (Germany), a research area of the Bayreuth Center of Ecology and Environmental Research (BayCEER). It is a FLUXNET (Baldocchi et al., 2001) site (DE-Bay) with carbon-dioxide flux measurement above the spruce forest since 1996 and intensive ecological and meteorological studies in this area (Matzner, 2004). The site is located NW of the upper EGER river valley (Fig. 1).

The site rates as one of the best of the European FLUXNET sites in terms of data quality. Regarding footprint classification, it is one of the good sites with more than 85 % of the flux originating from the target area “spruce”, with the remainder comprising areas of the clearing and some of the quarry (Göckede et al., 2008). It is an extensively investigated location with the good logistical conditions. At *Waldstein-Weidenbrunnen,* CarboEurope quality control tools have been developed. This included the use of *Waldstein-Weidenbrunnen* data sets for the comparison of eddy-covariance software (Mauder et al., 2008) and the test of the footprint classification scheme (Göckede et al., 2004, 2006, 2008; Rebmann et al., 2005). Many experimental efforts of the University of Bayreuth have been realized at our site, particularly a comprehensive micrometeorological experiment in 2003 (Thomas and Foken, 2007a), as well as the BEWA 2001 and 2002 field experiments (Klemm et al., 2006). The measurements for

many parameters of the FLUXNET data set started between 1992 and 1996 (Rebmann et al., 2004). Meanwhile, the *Waldstein-Weidenbrunnen* FLUXNET data set has been used in several publications and is partly available in the so-called La Thuile data set (http://www.fluxdata.org/). More detailed information of the site can be found in Gerstberger et al. (2004), recently updated by Staudt and Foken (2007) within the EGER project.

The dominating trees are Norway Spruce (*Picea abies*) with a canopy height of 25 m in 2008. Biometric data of the trees have been obtained by measurements of tree circumferences, tree positions (Forest Laser, Criterion Survey Laser Series 400, Laser Technology Inc., USA), and tree heights and crown lengths (inclinometer, Suunto, Finland). Horizontal distribution of Plant Area Index (PAI) was measured with two optical area meters (Plant Canopy Analyzer, LAI2000, LiCor, USA). This site inventory, available for the fenced area of the Waldstein-*Weidenbrunnen* site (1.3 ha), was used for the parameterization of the 3-D STANDFLUX model. The plant area index is $5.6 \pm 2.1\,m^2\,m^{-2}$ for the overstory trees (average and standard deviation of 532 measurements within the fenced area). The measured PAI was converted to LAI ($4.8\,m^2\,m^{-2}$) and SAI ($0.8\,m^2\,m^{-2}$) using allometric relations from inventory data gathered during IOP-1 and IOP-2 at the site. Two thirds of the fenced ground area is covered with bare litter or understory composed of mainly *Deschampsia flexuosa* and mosses, with an LAI of $0.5\,m^2\,m^{-2}$ and less. In the remaining third, open places with frequent sun spots are covered with *Picea abies* and *Vaccinium myrtillus*, with understory PAI of $3.5\,m^2\,m^{-2}$. The average vertical profile of the plant area index is given in Fig. 2 (average from 5 profile measurements).

Based on the PAI profile (Fig. 2), the turbulence structure within the *Waldstein-Weidenbrunnen* forest site appears to be similar to those observed at other sites: there, the measures of integral turbulence characteristics (σ_u/u_*, σ_v/u_*, σ_w/u_*; standard deviations of the horizontal, u, v, and vertical, w, wind components; u_*: friction velocity) typically decrease from their values observed in the surface layer (above the canopy = 100 %) to values between 15 and 40 % at 2 m above ground (Fig. 3, Amiro,

1990; Raupach et al., 1996). Inside the forest ($z < h_c$; z: height; h_c: canopy height) the parameterization proposed by Rannik et al. (2003) is nearly fulfilled (see Appendix A), which was used in the footprint model for the *Waldstein-Weidenbrunnen* site (Göckede et al., 2006).

Since 1994, meteorological data have been monitored at a clearing (*Waldstein-Pflanzgarten,* 50°08′35″ N, 11°51′49″ E, 765 m a.s.l.) about 200 m west of the *Waldstein-Weidenbrunnen* site. Corresponding climate data are given in Table 1, complemented by recent climatic trends. According to this classification, the *Fichtelgebirge Mountains* are located in the transition zone from maritime to continental climates. Since 1985 there has also been continuous monitoring of ambient O_3, NO, NO_2 and sulphur dioxide (SO_2) concentrations at the *Waldstein-Pflanzgarten* site (up to 1993 station *Wülfersreuth* of the Bavarian Environment Agency). Since 1985, median annual O_3 concentrations have ranged between 20 and 30 ppb, and median annual NO_x (= NO + NO_2) concentrations between 2 and 5 ppb. Those of sulphur dioxide have, since 1995, been less than 1 ppb (Foken, 2003; Lüers et al., 2009).

On 18 January 2007, shortly after the start of the EGER project the "hurricane like" low pressure system "Kyrill" destroyed large forested areas south of the *Waldstein-Weidenbrunnen* site (Fig. 4). Results of a footprint analysis performed for the conditions after "Kyrill" (Siebicke, 2008) are shown in Fig. 5, indicating that "Kyrill" related clearcuts are outside of the major footprint area. It can be assumed that the footprint of the target area "spruce" of *Waldstein-Weidenbrunnen* is not significantly affected.

2.2 Intensive Observation Periods (IOPs) of the EGER project

The first Intensive Observation Period (IOP-1) of the EGER project at the *Waldstein-Weidenbrunnen* site took place in September and October 2007, the second in June and July 2008 (IOP-2). Mainly wet autumn weather conditions characterized IOP-1, while sunny summer weather conditions with scattered showers prevailed during IOP-2. An overview of the meteorological conditions and ambient O_3, NO, NO_2, and SO_2 concentrations is given in Tables 2 and 3. Wet deposition of the ionic components of

rain (in mg m^{-2}), integrated over the entire time period of IOP-1 and IOP-2, was found to be typical for the region. Highest wet deposition rates were observed in the rain fall just after the "Golden Days" of IOP-1 and during the heavy rainfall on 3 July 2008 (IOP-2), respectively. Average O_3, NO, NO_2, and SO_2 concentrations, observed at 31 m (a.gr.) at the main tower were within the typical range of the long-term data (monitored at the *Waldstein-Pflanzgarten* site (3 m a.gr.). During IOP-2, maximum SO_2 and NO_2 concentrations (10.8 ppb and 15.1 ppb, respectively) occurred on 9 June 2008, when easterly air masses have reached our site from the industrialized regions of the Czech Republic.

Within the scope of this overview paper, we have selected for each IOP a so-called "Golden Days" period to present some of our results: 20 to 24 September 2007 (IOP-1) and 28 June to 2 July 2008 (IOP-2), respectively. These periods were characterized by high radiation, no precipitation and hardly any clouds (to emphasize photochemical aspects of our studies). The "Golden Days" period of IOP-2 was warmer and drier than that of IOP-1, with higher air and soil temperatures, higher maximum water vapour pressure deficits and lower soil moistures. Wind speeds were moderate and comparable for both "Golden Days" periods. While the year 2007 was the warmest in the region since permanent weather observations have started in Bayreuth (1850), the summer 2007 was warm but not extreme. IOP-1, starting just at the end of summer 2007, was always under influence of cyclonic conditions and it was only during the "Golden Days" that the anticyclone "Katrin" dominated Central Europe. From 18 June 2008 onward, IOP-2 (in the beginning cold and cyclonic) experienced warmer air, which was bordering colder air masses to the north. Under these warm and cyclonic conditions, thunderstorms passed through the *Fichtelgebirge* region including our site on 25 June (8.5 mm, 15:10–16:50 CET). The IOP-2 "Golden Days" period, starting on 28 June, was characterized by dry summer weather, not dominated by an anticyclone, and ended on 3 July with the cyclone "Renate" (44.1 mm of rain). Up to the end of IOP-2 cyclonic conditions (with some showers) returned.

2.3 Measurements

2.3.1 General set-up of towers and instrumentation

The so-called "main tower" (31 m, walk-up type) of the *Waldstein-Weidenbrunnen* site (see Fig. 6a, Table 4) served for standard meteorological measurements (e.g. vertical profiles of wind velocity, dry and wet bulb temperature) as well as for the measurements of vertical profiles of trace gas concentrations and trace gas fluxes. An additional, 35 m tall and slim tower for turbulence measurements was set up approx. 60 m south-east of the "main tower" (see Fig. 6b). This action was aimed to increase the data quality of micrometeorological in- and above canopy flux measurements in the footprint area of the *Waldstein-Weidenbrunnen* spruce forest (canopy height 23–25 m). 60 m northwest of the "main tower" another walk-up tower ("bio-tower") for plant physiological measurements was installed (see Fig. 6c). Along the NE-SW slope (approx. 3°) of the site, where catabatic flows could be expected, five 2 m high masts, equipped with sonic anemometers (not all masts) and intakes for CO_2 concentration measurements, were set up, while another six masts (identical instrumentation) were placed between the "bio-tower" and the "turbulence tower" perpendicular to the slope and along a small trail (for more details see Serafimovich et al., 2008a, b). During IOP-1, turbulent fluxes were measured at "main" and "turbulence" towers only; during IOP-2 a Modified Bowen-ratio system (Liu and Foken, 2001) was installed at the clearing north-east of the "turbulence tower" (50°08′30.32″ N, 11°52′11.0″ E, 780 m a.s.l.), close to the position of the mini-sodar, see Sect. 2.3.2).

2.3.2 Remote sensing measurements of the atmospheric boundary layer

In complex terrain like the *Waldstein-Weidenbrunnen* site, monitoring of the atmospheric boundary layer's structure became an important tool for interpretation of the turbulent exchange data. For this monitoring a composite of several remote sensing instruments was used: a sodar/RASS and a mini-sodar system at the field site, a

482 MHz-windprofiler of the German Meteorological Service about 25 km south of the field site, and a 2D sonic anemometer at the top of the "main tower" (Table 5). Data from the two sodar systems and the sonic anemometers at the "turbulence tower" were also used to investigate coherent structures in both the canopy and the atmospheric boundary layer (Thomas et al., 2006).

2.3.3 Measurements of turbulent fluxes

As shown in Table 6, six levels of the "turbulence tower" and up to four levels of the "main tower" have been equipped with 3D sonic anemometers, most of them also with fast-response open-path CO_2 and H_2O analyzers, some of them with fast-response O_3 analyzers, and one level (IOP-2) with the intake for fast-response measurements of NO and NO_2 concentrations. The EUROFLUX methodology (Aubinet et al., 2000) and recent updates of the TK2 software (Mauder and Foken, 2004; Mauder et al., 2008) provided the basis of all calculations for the turbulent fluxes of momentum, sensible heat, latent heat, CO_2, O_3, NO, and NO_2. Furthermore, all flux measurements for the *Waldstein-Weidenbrunnen* site were footprint controlled (Foken and Leclerc, 2004; Göckede et al., 2004, 2006) and data quality checked (Foken and Wichura, 1996; Foken et al., 2004). The coordinate system for all 3-D wind measurements was chosen parallel to the stream lines using the planar-fit method (Wilczak et al., 2001). This was also the basis for determining advection through adaptation of the concept by Aubinet et al. (2003).

During IOP-1, only the turbulent O_3 flux was measured, but during IOP-2 turbulent fluxes of NO, NO_2, and O_3 were measured using eddy-covariance systems. In case of NO and NO_2, high frequency (5 Hz) time series of NO and NO_2 concentrations were recorded with a specialized, fast-response, state-of-the-art, high precision 2-channel NO-NO_2 chemiluminescence analyzer (model CLD 790SR-2, Ecophysics, Switzerland). While one channel was used for the direct measurement of the NO concentration, the measurement of the NO_2 concentration was indirect, following high efficiency conversion of NO_2 to NO (through two up-stream solid state blue light converters

in series) and consecutive NO detection in the second channel of the chemiluminescence analyzer. To maintain continuous time series of the fast-response NO and NO_2 measurements, NO and NO_2 signals have not been calibrated on-line; instead, they have been related to NO and NO_2 concentrations which were measured side-by-side by slow-response NO-NO_2 chemiluminescence analyzers (see Sect. 2.3.3). During IOP-1 and IOP-2, these analyzers revealed detection limits (3σ-definition) ranging between 0.05–0.12 ppb (NO) and 0.22–0.76 ppb (NO_2), respectively; data found to be below the limit of detection have been discarded. A sonic anemometer (CSAT3, Campbell Scientific Inc., USA) was used to measure fluctuations of the 3-D wind velocities at 20 Hz. A 53 m long insulated bundle containing the Teflon inlet tubes, tube heating as well as interface cables from the data logger ran from the top of the "main tower" to the analyzer and control computers in a nearby air-conditioned shelter (container). In the case of O_3, high frequency (20 Hz) time series of O_3 concentration were recorded by fast-response solid-phase chemiluminescence analyzers (Güsten and Heinrich, 1996) designed by different manufacturers (s. Table 6). Sonic anemometers were deployed next to the O_3 analyzers (s. Table 6). Combining the signals of 3-D wind velocity fluctuations with those from the fast-response O_3-analyzers provided turbulent O_3 fluxes above (IOP-1, IOP-2) and, within (IOP-2), the *Waldstein-Weidenbrunnen* spruce forest. Solid-phase chemiluminescence analyzers provide O_3 concentration only in relative units (voltage), and the analyzers' sensitivity is not temporally constant (due to the influence of relative humidity on the chemiluminescent dye). However, absolute O_3 concentrations were simultaneously measured side-by-side each fast-response O_3-analyzer by UV-absorption based ozone analyzers (see Sect. 2.3.3). Based on these data, fast-response O_3 signals could be converted to O_3 concentration and hence, after applying the above mentioned procedures for correction and quality check of eddy-covariance measurements, the turbulent O_3-fluxes and deposition velocities were calculated.

2.3.4 Profile measurements

Measurements of the vertical profiles of wind speed and dry and wet bulb temperatures are part of a standard and continuously running monitoring programme at the *Waldstein-Weidenbrunnen* site (www.bayceer.de). Cup anemometers, characterized by low distance constant (approx. 3 m), and Frankenberger type psychrometer (Frankenberger, 1951), all equipped with high precision sensors, have been mounted at different levels along the "main tower" (s. Table 7). During both IOPs, these sensors (system I, see Table 7) have been amended by additional wind speed sensors (A100ML, Vector Instr., UK) and home-built, thermocouple-based psychrometers (system II, see Table 7).

Along the "main tower", vertical profiles of CO_2, H_2O, NO, NO_2, and O_3 concentrations were measured at nine (IOP-1) and eleven (IOP-2) levels, respectively (see Table 7). Due to the limited absolute accuracy (but generally much better precision) of the trace gas analyzers, concentrations from different levels have been measured sequentially by one set of analyzers in order to resolve even small vertical differences of concentrations. To keep the time period required to "scan" the full profile short (<30 min), two identical but independently operating sets of analyzers have been deployed. One set was applied to levels of the upper part of the profile (>24 m, IOP-1; >16.5 m, IOP-2), the other set for the lower levels of the profile (i.e. within canopy and particularly close to the soil–trunk space interface). Both sets of analyzers had overlapping levels (24 m, IOP-1; 16.5 m, IOP-2), where concentration measurements (from side-by-side intakes) provided a continuous data set to cross-check (and to correct) for systematic offsets. Ambient air was drawn from the different intake levels through heated and insulated PTFE-tubing (4.1 mm inner diameter; opaque; length: 55 m each) into an air-conditioned container (housing the two sets of analyzers) on the forest floor close to the "main tower". All sampling lines were continuously purged, and the "active" sampling line was sequentially switched between the different levels (switching interval: 1.5 min). NO and NO_2 concentrations were measured by 1-channel chemiluminescence analyzers (CLD TR780, Ecophysics, Switzerland). NO was detected first,

then NO_2, after the sampling air has passed a solid-state blue light converter (installed upstream from the analyzer for species specific conversion of NO_2 to NO). Detection limits (3σ) for NO and NO_2 during the experiments were <0.12 and <0.76 ppb, respectively. Precision was <0.6 % (10 ppb NO) and <4 % (20 ppb NO_2), respectively. For measurements of O_3 concentrations, UV absorption spectrometers (TEI 49c/I, Thermo Electron, USA) which had a precision <2 % were used. Concentrations of CO_2 and water vapour were measured by NDIR absorption analyzers (Li7000 and Li840, LI-COR Biosiences, USA); corresponding precision was <0.2 % for both CO_2 and H_2O. All analyzers were calibrated at least weekly, using certified CO_2 standards (pressurized cylinders), a dew point generator (Li-COR Biosiences, USA), and a certified NO standard (5 ± 0.09 ppm, Air Liquide, Germany) in combination with a gas-phase-titration unit (model 146c, Thermo Electron, USA) to generate suitable concentrations of NO, NO_2, and O_3.

During IOP-1, concentrations of the NH_3-HNO_3-NH_4NO_3 triad were measured at two heights above the forest canopy using a novel wet chemical instrument, the GRAEGOR (GRadient of AErosols and Gases Online Registrator, Thomas et al., 2009). Gaseous NH_3 and HNO_3 and particulate NH_4NO_3 constitute a thermodynamic equilibrium which strongly depends on relative humidity and temperature as well as on aerosol composition, especially SO_4^{2-} concentrations (Mozurkewich, 1993; Nenes et al., 1998; Stelson and Seinfeld, 1982). GRAEGOR is capable of measuring the interacting species gaseous NH_3 and HNO_3 as well as particulate NH_4^+, NO_3^-, and SO_4^{2-} selectively and simultaneously at two different heights. For the first time, such highly time resolved measurements of the complete triad were performed above a forest canopy. The instrument was thoroughly characterised for its ability to resolve vertical concentration differences above the forest (and a grassland site) for a range of atmospheric conditions (Wolff et al., 2010a). From the experimentally determined errors of the concentration differences the resulting flux errors were estimated. For the *Waldstein-Weidenbrunnen* forest experiment median instrumental flux errors were: 50 % (NH_3), 38 % (HNO_3), 57 % (NH_4^+), and 68 % (NO_3^-), respectively (Wolff et al., 2010a).

During both IOPs, ambient HONO mixing ratio were measured with a wet-chemical instrument, the Long Path Absorption Photometer (LOPAP, Kleffmann et al., 2002; Heland et al., 2001). This underlying technique offers a high temporal resolution (5–7 min) and a very low detection limit of about 0.001 ppb. During IOP-1, we had set up two LOPAP instruments, one close to the forest floor (0.5 m) and the other one just above the canopy (24.5 m). The data set provides valuable information to study potential HONO formation processes on the different surfaces, which may be heterogeneous or even photo-enhanced sources of HONO.

Though corresponding data are not reported here, it should be mentioned (for the sake of completeness of the EGER overview) that the above-mentioned measurements of turbulent fluxes and vertical profiles were complemented by measurements of the soil-atmosphere exchange of CO_2, ^{220}Rn, and ^{222}Rn (static chamber), NO, NO_2, and O_3 (dynamic chambers), measurements of the plant-atmosphere exchange of CO_2, H_2O, NO, NO_2, and O_3 (dynamic branch/twig cuvettes), as well as by laboratory incubation measurements of biogenic NO emission from soil samples taken from plots of the *Waldstein-Weidenbrunnen* site covered by different understory vegetation (moss, grass, blueberries, young spruce, see Bargsten et al., 2010).

2.4 Scale and coupling analysis

As stated in the introduction, the experimental and also the modelling design of the EGER studies was based on the analysis of the spatial and temporal scales of the relevant exchange processes in the forest, atmosphere, plants and soil. The temporal scales were thereby compared with the characteristic chemical reaction time and the time scales of coherent structures. Furthermore, the coupling between the atmosphere and the canopy was taken into account. In the following the basics of these methods of investigation are briefly presented.

2.4.1 The scale problem

The physical, chemical and biological processes controlling the exchange of energy and trace substances are characterized by time scales extending from femto-seconds (e.g. electron transport in chloroplasts), over several hours (e.g. horizontal advection), to several years (climate, Beniston, 1998), and by spatial scales ranging from a few micrometers (e.g. reactions of heterogeneous chemistry) to the size of landscape elements (about $10 \times 10\,km^2$). Investigations of the EGER project are focussing on widely overlapping scales (Jarvis, 1995) from contributions of the individual physical, chemical and biological processes, whereas our measuring and modelling techniques are related to specific scales.

The extent of the scale problem is illustrated in Fig. 7, where spatial and temporal scales of atmospheric, biological, soil and chemical processes, which control the exchange of energy and trace substances, are schematically shown. Within the entire range of atmospheric processes (light blue squares, ranging from micro scale γ to meso scale α, as defined by Orlanski, 1975), the scales concerning the exchange processes of energy, water, and trace substances comprise (i) turbulent transport in canopies (white star), (ii) advection in canopies (white circle), (iii) turbulent transport above canopies (white diamond), (iv) coherent structures in and above canopies (blue double arrow), (v) footprint related turbulent fluxes (white square), and (vi) horizontal advection at canopy top (white triangle). In Fig. 7, the typical scales of processes in plants (Schoonmaker, 1998), those in soil (Vogel and Roth, 2003), in the saturated and unsaturated zone (Blöschl and Sivapalan, 1995) are shown by the brown framed, spotted area. While there is a broad overlapping of the spatial and temporal scales of plant and soil processes, there is only a marginal overlapping of these with the scales of atmospheric processes; with increasing time scales, atmospheric processes separate more and more from plant and soil processes with regard to space. Not included in Fig. 7 are spatio-temporal scales of the measuring techniques from plant enclosures and soil chambers (a few tenths of square metres) to eddy-covariance data

with a footprint up to some square kilometres. Remote sensing techniques have even larger areas, depending on the height from where the signal originates. Note that coherent structures have a significantlylarger length scale in the vertical than in the horizontal direction, and time scales are also longer. This important issue was recently underlined by Mahrt (2010) regarding the averaging technique for eddy-covariance measurements.

Gas-phase and heterogeneous reactions of relevant reactive trace gases (see reactions 1–15 in Fig. 7) are only attributed to corresponding temporal scales (1/e reaction times). These characteristic chemical time scales (see Dlugi, 1993) simply result from ambient concentrations of the reaction partners, reaction kinetics or thermodynamic equilibrium considerations, and (photo-) chemical constants or variables. However, most of the corresponding (photo-)chemical constants have been derived from laboratory experiments in well-mixed reaction chambers (see Atkinson et al., 2004). Therefore, corresponding spatial scales (most likely $<<1$ mm) seem not to be relevant for real atmospheric conditions, particularly not within tall canopies, where (strong) decoupling by vertical thermodynamic stratification is (at least during night) more likely than full coupling with the (above canopy) surface layer, or even complete turbulent mixing throughout trunk and canopy spaces. The latter, however, is the prerequisite of corresponding volume averaging of chemical processes, which is a volume averaging of soil and plant processes – the basis of coupling of turbulent, soil, plant, and chemical processes.

2.4.2 The Damköhler number

As already mentioned in Sect. 1, the Damköhler number (DA) is the ratio of two particular time scales, namely the characteristic turbulent transport time (τ_{turb}) over the characteristic chemical time scale (τ_{chem}):

$$DA = \frac{\tau_{\mathrm{turb}}}{\tau_{\mathrm{chem}}} \tag{1}$$

Dominance of the turbulent transport over chemical reaction (hence, treating a trace substance as "non-reactive" during transport through the forest or considering a trace substance as "non-reactive" for "volume averaging") is given, if $DA \leq 0.1$. Defined by the K-approach, the characteristic turbulent time scale, τ_{turb}, may be computed from the mean transfer velocity v_{t} and the thickness Δz of the layer being considered (Mayer et al., 2011)

$$\tau_{\mathrm{turb}} = \frac{\Delta z}{v_{\mathrm{t}}} \tag{2}$$

The final expression for the time scales of turbulent trace gas transport thus reads:

$$\tau_{\mathrm{turb}} = \frac{\Delta z^2 \varphi_H(\zeta) \cdot Sc_{\mathrm{t}}}{\kappa \cdot z_{\mathrm{m}} \cdot u_*} \tag{3}$$

with φ_H the universal function for the heat exchange (also used for trace gases), $\zeta = z/L$ with the Obukhov-length L, the von-Kármán-constant κ, the measuring height z_{m}, the turbulent Schmidt number Sc_{t}, and the friction velocity u_*. It should be stated that Eq. (3) is only applicable under Monin-Obukhov similarity conditions.

Typical time scales for reactions of chemically reactive compounds are given in Fig. 7 (Reactions 1–15, see Dlugi, 1993). However, assuming reasonable vertical mixing and considering given (measured) concentrations of reaction partners, the characteristic chemical reaction times can be calculated using (i) kinetic constants (Atkinson et al., 2004), (ii) radiation fluxes for photolysis (e.g. for O_3, NO_2, and HONO), and (iii) known thermodynamic quantities, NH_3-HNO_3-NH_4NO_3, (see Wolff et al., 2010b), respectively. As in Mayer et al. (2011), in the following we consider for the chemical timescale (τ_{chem}) only the NO–NO_2–O_3 triad including the (photo-) chemical reactions $O_3 + NO \rightarrow NO_2 + O_2$, characterized by the reaction coefficient $k_1 = 1.40 \times 10^{-12} \exp^{-1310/T}$ (see Atkinson et al., 2004) and $NO_2 + h\upsilon \rightarrow NO + O_3$ ($\lambda < 420$ nm, characterized by the NO_2 photolysis frequency $\boldsymbol{j}(NO_2)$, which has been measured directly). The chemical destruction of NO_2 is then controlled by $\boldsymbol{j}(NO_2)$ only and, in turn, the chemical production of NO

and O_3. From simple reaction kinetics, the time scales for NO, NO_2 and O_3 are given by $\tau_{NO} = (k_1 N_{O3})^{-1}$, $\tau_{NO2} = (\boldsymbol{j}(NO_2)^{-1}$, and $\tau_{O3} = (k_1 N_{NO})^{-1}$ (where N_{NO} and N_{O3} represent the molecule number density of NO and O_3). The overall chemical timescale of the NO–NO_2–O_3 triad (τ_{chem}), a measure of the extent of chemical conversions (for comparison with the turbulent time scale τ_{turb}), has been formulated by Lenschow (1982):

$$\tau_{chem} = \frac{2}{\sqrt{(j(NO))^2 + k_1^2 (N_{O_3} - N_{NO}) + 2k_1 j(NO_2)(N_{O_3} + N_{NO} + 2N_{NO_2})}} \quad (4)$$

2.4.3 Coupling between the atmosphere and the ecosystem

The coupling between the atmosphere and the canopy is related to the development of the mixing layer, which for the *Waldstein-Weidenbrunnen* site has already been studied in detail (Thomas and Foken, 2007a; Wichura, 2009; Wichura et al., 2004). For the *Waldstein-Weidenbrunnen* site the characteristic length scale of the mixing layer

$$L_S = \delta_w/2 = \frac{u(z_B)}{(\partial u/\partial z)_{z=z_B}} \quad (5)$$

was found to be on the order of 7–8 m in day time and 6–7 m in night time except in the SE sector where it was only 5 m. Therefore, with the wavelength of the initial Kelvin-Helmholtz instability Λ_x a linear relation exists between both scales (Raupach et al., 1996)

$$\Lambda_x = m\, L_s, \quad (6)$$

The coefficient m ranged from 7–10 and for the SE sector up to 16 (Thomas and Foken, 2007a). This was found in 2003 for a canopy height of about 19 m. Following the determination of the thickness of the roughness sublayer according to Verhoef et al. (1997) $z* = h_c + cL_s$ with $c = 2\ldots3$, it follows for the *Waldstein-Weidenbrunnen* site that approx. $z_* = 40$ m and for the present canopy height about 50 m and in the SE

sector even less. This is much lower than for other sites (Mölder et al., 1999), probably because of the special location near a ridge.

The wavelength of the initial Kelvin-Helmholtz instability is also necessary to determine the flux contributed by coherent structures between different layers in the canopy and atmosphere (Thomas and Foken, 2007b). Thereby the coherent structures were detected with a wavelet tool (Thomas and Foken, 2005). On this basis an exchange classification was proposed, and a brief description is given for the five exchange regimes:

Wave motion (Wa). The flow above the canopy is dominated by linear wave motion rather than by turbulence (Thomas and Foken, 2007a; Cava et al., 2004).

Decoupled canopy (Dc). The air above the canopy is decoupled from the canopy and subcanopy.

Decoupled subcanopy (Ds). The atmosphere is coupled with the canopy, but decoupled from the subcanopy. The region of coherent exchange is limited to the canopy.

Coupled subcanopy by sweeps (Cs). The exchange between the above-canopy air and the subcanopy is forced by the strong sweep motion of coherent structures only.

Fully coupled canopy (C). The atmosphere, the canopy and the subcanopy are in a fully coupled state.

2.5 Aerodynamic method and roughness sublayer

For many trace gases the use of the eddy-covariance technique is not yet feasible due to the lack of fast response sensors. In our case for the GRAEGOR measurements of gaseous NH_3 and HNO_3 and particulate NH_4NO_3 with a sampling time of 30 min

(Wolff et al., 2010a) the application of the flux gradient similarity (Monin-Obukhov similarity) was a useful tool. From integration of flux-gradient equations between two levels follows the aerodynamic method for the trace gas flux (Foken, 2008b; Monteith and Unsworth, 2008):

$$F_c = -\frac{\kappa^2 (u_2 - u_1)(c_2 - c_1)}{\{\ln[(z_2 - d)/(z_1 - d)]\}^2} (\Phi_m \Phi_c)^{-1} \quad (7)$$

This equation was already formulated for the application above a canopy with the zero-plane displacement height d. Furthermore, for the integrated universal functions $\Phi_{m,c}$ the use of the universal function according to Businger et al. (1971) in the modification by Högström (1988) is recommended (Foken, 2008b; Jacobson, 2005). The function Φ_c already contains the turbulent Prandtl number (Foken, 2006) and therefore, with $Pr_t \sim Sc_t$, Eq. (7) was formulated without the turbulent Schmidt number.

According to the definition of the profile functions in the roughness sublayer, the integrated universal function of the roughness sublayer must be included in the profile function for scalars and momentum and therefore both must be included in Eq. (7). While the integrated universal function for the roughness sublayer for momentum is known, this function is missing for scalars because of the lack of a suitable experimental control.

Because of all these deficits a very pragmatic method was chosen for the application of the aerodynamic method. The enhancement factor for scalars was assumed to be $1/\varphi_c^*(z/z_*) \approx 1$.

Instead of using an enhancement factor for momentum, the friction velocity was directly determined with eddy-covariance measurements at the relevant height of the application of the aerodynamic method. With this assumption it follows for Eq. (7)

$$\overline{w'c'} = -\frac{\kappa u_* (c_2 - c_1)}{\ln[(z_2 - d)/(z_1 - d)]} \Phi_c^{-1} \quad (8)$$

Therefore, an unknown error due to the enhancement factor for scalars must be assumed which underestimates the fluxes up to 30–60 %, if the enhancement factor for

scalars is in the same order as that for the momentum exchange (Mölder et al., 1999). On the other hand similar errors must be assumed for the universal function for scalars and the turbulent Prandtl and Schmidt numbers (Högström, 1996). Probably the error increases because the turbulent Prandtl number used by Högström (1988) was very high (Foken, 2006).

2.6 Modelling

The ACASA model (Advanced Canopy-Atmosphere-Soil Algorithm, Pyles, 2000; Pyles et al., 2000) is a multi-layer model that incorporates a third-order closure method to calculate turbulent transfer within and above the canopy (Meyers, 1985; Meyers and Paw U, 1986, 1987). Such a higher order closure method overcomes the limitations of turbulence modules found within many stand-scale models that apply the flux-gradient relationships (K-theory) within forest canopies (Denmead and Bradley, 1985; Shaw, 1977). Important features of the ACASA model are: long- and shortwave radiative transfer within the canopy (Meyers, 1985), the calculation of leaf, stem and soil surface temperatures using the fourth-order polynomial of Paw U and Gao (1988); plant physiological response to ambient conditions by the use of a combination of the Ball-Berry stomatal conductance (Leuning, 1990; Collatz et al., 1991) and the Farquhar and von Caemmerer (1982) photosynthesis equation following Su et al. (1996) and a soil module adapted from MAPS (Mesoscale Analysis and Prediction System, Smirnova et al., 1997, 2000)

The model STANDFLUX (Falge et al., 1997, 2000) provides a framework for integrating three-dimensional aspects of forest stand structure and light interception, one-dimensional vertical aspects of stand microclimate, and gas exchange behaviour of plant organs distributed throughout a forest stand. It consists of three nested components with a leaf or branch gas exchange module at the innermost level (for needled portions of branches), a three-dimensional single-tree light interception and gas exchange module as the next step in the hierarchy, and a three-dimensional forest-stand gas exchange model occupying the outermost shell. The model structure is designed

for separate validation at each organizational level. Predicted net photosynthesis and conductance of foliage elements (for spruce needled branch ends) can be compared with dynamic cuvette gas exchange measurements and simulated single tree transpiration results with xylem sap flow estimates, while stand level predictions may be validated via eddy-covariance measurements.

Results from measurements of a portable gas exchange system (GFS3000, Walz, Effeltrich, Germany) enabled us to parameterize the response of needle CO_2 and H_2O exchange under assorted micrometeorological factors during the field campaigns. Parameters for a leaf gas exchange model (Farquhar type) were derived, utilizing information from both single factor dependencies on light, temperature, CO_2 concentration, and relative humidity, and diurnal time course measurements of gas exchange.

3 Results and discussion

The following sections concentrate on two fair weather periods in both IOPs, namely 20–24 September 2007 (fall, DOY 263–267, IOP-1), and 29 June–2 July 2008 (summer, DOY 181–184, IOP-2). Both periods were characterized by high and nearly identical radiation fluxes, no precipitation, hardly any clouds and very similar wind forcing. This facilitates the comprehensive interpretation of our first results, particularly with respect to photochemical aspects.

3.1 Roughness sublayer

The procedure used to characterize the roughness sublayer (described in Sect. 2.5) could not be realized for the *Waldstein-Weidenbrunnen* site, because none of the EGER towers were tall enough to install a sufficient number of measurement levels between the top of the canopy (23–25 m a.gr.) and the roughness sublayer height z_* (presumably >50 m a.gr.). Data from the sodar/RASS and the mini-sodar cannot be used because their (large) footprint is not representative for the *Waldstein-Weidenbrunnen*

forest. Therefore, we preferred using the following alternative to derive the desired correction function $\varphi_*(z/z_*)$. The function φ_* has been determined from data obtained during the recent field experiment COPS (Wulfmeyer et al., 2011), performed over a growing maize field (for details see Eigenmann et al., 2009).

In Fig. 8 the results of the COPS experiment over maize are shown in comparison with the data from the Waldstein-Weidenbrunnen site (only in the range $z/z_* = 0.41$–0.45) and the equations

$$\varphi_*(z/z_*) = \exp[-0.7(1 - z/z_*)] \quad (9)$$

(Garratt, 1992) and

$$\varphi_{*_u} = \left(\frac{z}{z_*}\right)^{\eta} \quad (10)$$

(Cellier and Brunet, 1992). A strong dependence on the friction velocity was found, but for moderate friction velocities up to 0.6 m s^{-1}, Eq. (10) gives the best approximation with $\eta = 0.6$, which was also found by Mölder et al. (1999). A slight but not significant dependence on stability was also recognised. The enhancement factor for the momentum exchange at 31 m height is therefore approximately 1.6.

Similar to other authors (Mölder et al., 1999), the number of measuring points and the accuracy of the data were not adequate for the calculation of the universal function of the roughness sublayer for scalars. For the temperature profile over the maize field a linear relationship with $\eta = 1.0$ was in agreement with Mölder et al. (1999). At the forest site the scalars at a height of 23 m, at the top of the canopy, already showed an increased gradient to the top of the tower and no reduced gradient according to the roughness sublayer assumption. Therefore, for scalars no additional enhancement factor should be used (see Sect. 2.5).

3.2 Coherent structures – coupling between the atmosphere and canopy

The method described in Sect. 2.4.3 was also used to separate the flux into a Reynolds averaged flux and a flux transported by coherent structures (upper panel in Fig. 9). It

was found that momentum and sensible heat transport by coherent structures is dominant in the canopy and carbon dioxide and latent heat transport by coherent structures increases with height within the canopy and reaches a maximum at the upper canopy level. The flux contribution of the ejection and sweep phase of coherent exchange were also determined. The flux contribution of the ejection phase decreases with increasing height within the canopy and becomes dominant above the canopy level. The flux fraction transported during the downward directed sweep phase increases with height within the canopy and becomes the dominating exchange process at the upper canopy level. Close to the ground surface in the subcanopy space, ejection and sweep phase contribute equally to the flux transport. This issue is discussed in more detail by Serafimovich et al. (2011). Furthermore Fig. 9 shows the coupling classification and, for a better understanding, also selected meteorological parameters and fluxes

Conditional sampling analysis shows a domination of coherent structure signatures in vertical wind measurements (Fig. 10) with probable temporal scales in the range 10 s to 40 s. The number of coherent structures detected at the turbulence tower is lowest directly under the crown (5 m) and higher in the trunk space and above the canopy with a maximum at the canopy level. Most of the structures were found in the vertical wind velocity followed by the temperature. There were more structures found in water vapour flux than in carbon dioxide flux.

The analysis was extended to the lower boundary layer according to Thomas et al. (2006) using sodar measurements. To derive characteristics of coherent structures from sodar/RASS individual soundings, data preparation and the wavelet analysis were used. Due to the effect on the measurements of occasional environmental noise detection and discarding of erroneous data, gap filling and de-noising were applied (Crescenti, 1998; Miller and Rochwarger, 1970; Neff and Coulter, 1986). In a first step, the data were filtered using the error flag output by the sodar/RASS system. As a next step, a quality control described in Thomas et al. (2006) was applied. An example of the spectra of wavelet variance for different observation levels is presented in Fig. 11. The data for the lower observation heights exhibit the first maximum at ∼30 sec, whereas

the observation levels above show the stronger maximum at ∼50–60 sec.

The classification of the coupling was used in the following sections for a better understanding of the chemical processes. The first analysis showed that the attribution of coupling states into the classes C and Cs as well as W and Dc is difficult. Therefore the coupling classes C/Cs and W/Dc were combined to show a more significant picture of the results. First the statistics of the coupling classes is shown in Fig. 12 for both IOPs.

The typical difference between IOP 1 and 2 is the domination of class W/Dc in the autumn IOP-1 whereas in the summer IOP 2 in the same hours the case Ds is dominating. But the cases of well coupled situations are not significantly different for both IOPs. The typical asymmetry in the stability with stronger unstable situations in the morning, already stable situations in the afternoon and the strongest stable situation in the first half of the night can easily be seen in the distribution of the coupling classes as well (see Fig. 9). Obviously, IOP 2 shows an oasis effect (necessary energy of evaporation is on the cost of sensible heat flux, see Stull, 1988) with a stronger decoupling already in the hours 15–18 which is usually expected not to occur before the hours 18–21 (e.g. IOP-1). Situations with a good coupling were found in the nights of both IOPs, probably connected with low-level jets and gravity waves (see Sect. 3.3).

The analysis of coherent structure was also used to apply a relaxed eddy accumulation conditional sampling to determine the daytime soil respiration from turbulence measurements above the canopy. The method based on quadrant analysis (Shaw et al., 1983) with regard to CO_2 and water vapour contents can be used for identifying the origin of CO_2 fluxes (Scanlon and Albertson, 2001): this method was improved for a practical application and applied for different canopies by Thomas et al. (2008). However, for the dense *Waldstein-Weidenbrunnen* spruce forest corresponding results were not very satisfactory. Therefore the method was again tested during IOP-1 with some site specific modification for the conditional sampling characteristics. For the *Waldstein-Weidenbrunnen* satisfactory results were achieved leading to an integrated five-day flux.

In Serafimovich et al. (2011) the vertical coupling according to Fig. 9 was investigated as well as the horizontal coupling between the small towers in the trunk space used for advection investigation. This coupling concept was applied to advection investigations (Siebicke, 2011). The coupling was found to be much stronger along this trail (no understory) and not along the slope (understory up to 1 m height).

Although advection is very important for the carbon balance of a forest (Finnigan, 2008), the problem posed by measurement of the advection has still not been solved. The classical approach with a more or less steady-state flow through a volume element was, in many experiments, unsuccessful (Aubinet et al., 2010; Aubinet, 2008; Feigenwinter et al., 2008). This was also tested on the *Waldstein-Weidenbrunnen* site in 2003 and during both IOPs. Even very careful analysis of the data including a planar fit analysis (Wilczak et al., 2001) adapted to the process could not make the necessary progress. Therefore Siebicke (2011) tried to explain the measured horizontal carbon dioxide gradients along both tower lines with the complicated structure of the canopy and understory. He found significant correlations between the horizontal gradients, which were measured during IOP-2 with a high time resolution, and the duration and intensity of coherent structures.

3.3 Influences of the atmospheric boundary layer

To understand influences of the dynamics of the atmospheric boundary layer on surface exchange processes, information about the spatio-temporal behaviour of the boundary layer's temperature and wind fields must be known. The two installed sodar systems at the experimental site (see Sect. 2.3.2) showed a good agreement at those heights, which are covered by both systems. Also, upper levels of sodar and windprofiler measurements showed only very small differences. Therefore, the results of the three systems were combined to make available a composite picture of the boundary layer structure.

The specific aim of the investigation was the flow characteristics in the roughness sublayer and potential influences of the clear-cut south of the *Waldstein-Weidenbrunnen* site on trace gas fluxes. For stronger winds, the wind direction of the entire boundary layer dominates down to the canopy level. In contrast, Fig. 13 shows the influences of the clear cut on the wind field at the site. These situations (cloudy conditions) are related to very small horizontal wind velocities above the canopy and significantly lower vertical wind velocities (not shown). In general the main wind directions – in the south-west sector – are nearly identical at 200 m (sodar) and 1050 m (windprofiler) heights. A strong SE component, coming up the Lehestenbach valley, could occur as well, but only below 100 m at night.

Furthermore, the low-level jets (LLJ) found in 2003 were investigated more carefully and found to be similar to those in other studies (Banta et al., 2002). They were selected when the wind velocity above and below the jet was at least 2 m s^{-1} lower (Stull, 1988) and the duration of the jet was longer than 90 min. An example of this is shown in Fig. 14. The wind velocity of the jet was found to be above 10 m s^{-1} for about 6 h at a height of 300 m, decreasing up to 200 m. The wind direction of the jet was SE while above the jet the wind direction moved from SE over S to W. In the jet the vertical wind was negative. During IOP-1 LLJs were found on nine nights, mainly at about 150 m height with a typical wind velocity of 9 m s^{-1}. During the summer IOP-2 LLJs were found on 11 nights but typically at 250 m height with about 10 m s^{-1}.

Low level jets have a significant influence on the night-time exchange of a forest. Karipot et al. (2008, 2005) found that low-level jets enhance turbulence and mixing close to the ground due to increased shear. CO_2 fluxes are very small during calm periods following early evening hours and large fluxes are observed corresponding to the LLJ periods. The flux increases up to 9–15 µmol m^{-2} s^{-1}, though the u_* values increased only just above 0.2 m s^{-1}. This is an indication that during intermittent turbulent periods associated with features such as sporadic jets, high fluxes are possible from the large fluctuations in the accumulated CO_2, in phase with moderate vertical velocity fluctuations. CO_2-rich ejections from the canopy contribute more to the positive

flux during weak-LLJ events. For the LLJ shown in Fig. 14 similar conditions (Karipot et al., 2005, 2008) were found with an increase of the friction velocity and of the carbon dioxide flux from 4 µmol m^{-2} s^{-1} to 8 µmol m^{-2} s^{-1}.

The vertical distribution of the concentrations of NO, NO_2, O_3 and CO_2 is shown in Fig. 15 for the situation with the Low-Level-Jet (Fig. 14). Due to the increased shear a better mixing was found during the period with the LLJ between 02:00 and 08:00, with a maximum at 04:00. The better mixing resulted – for all trace gases – in a reduction of the accumulated concentrations near the surface (Fig. 15). In the early morning, at approximately 04:00, when the LLJ occupied lower heights, the atmosphere close to the surface is suddenly mixed with high NO_2 concentrations, probably an outflow of the upper Eger river valley during easterly winds. However, this picture contains some other features. The most impressive is the inflow of fresh air with low NO_2 and high O_3 between 22:00 and 24:00, connected with gravity wave influences. For high NO (and (NO_2) concentrations during the morning hours (06:00–12:00), see next Sect. 3.4.

3.4 Local advection of reactive trace gases

Concerning the interpretation of fluxes and vertical concentration gradients of the reactive NO-NO_2-O_3 triad, the *Waldstein-Weidenbrunnen* site shares a rather general problem with any other site located in polluted, but also in rural areas: the proximity to anthropogenic sources of NO_x (industrial, domestic and/or traffic). Within the dispersion plume close to these sources, freshly emitted NO of high concentration (several hundreds of ppb) titrates ambient O_3 and starts the formation of NO_2. However, it depends upon the day/night situation, on the actual boundary layer stability regime, and above all on the distance of the site to the source, to what extent flux and concentration gradient measurements will be biased by advection of high NO (or NO_2) concentrations. In the case of the *Waldstein-Weidenbrunnen* site, the unavoidable NO source consists of the nearby district road (HO18), characterized by a rather high traffic volume of 2100 cars per day (working days). The nearest distance of HO18 to the site is about

1.2 km. However, since main wind sectors of the site are SW to NW, and HO18 runs west of the site from SSE to NNW, "advective disturbance" of desired homogeneous concentration fields is more than likely. Exemplarily for the entire periods of IOP-1 and IOP-2, NO concentrations, measured with 5 Hz resolution (s. Sect. 2.3.2) above the canopy (30 m a.gr.), have been averaged to 30 min means and are shown for the "Golden Days" period of IOP-2 in Fig. 16. NO concentrations are observed every day to increase strongly at 06:00, reaching maximum values around 09:00, and to decline to <0.1 ppb after noontime. The early morning increase can definitely be attributed to the emission and subsequent accumulation of NO in the still existing shallow nocturnal boundary layer over the site with the begin of the commuting traffic (to district capitals Hof and Bayreuth) which starts at 05:30–06:00. Until 09:00, high NO concentrations (30 min averages) are associated with large standard deviations, indicating high variability and consequently low stationarity of NO concentrations. Although not shown here, mean NO_2 and O_3 concentrations also reveal large standard deviations. Noticeable growth of the daytime convective boundary layer (after 10:00) leads to substantial dilution of traffic emissions and consequently to much lower NO concentrations at the site. Following our sodar/RASS measurements, the convective boundary layer at the site is still present until 18:00–19:00; most likely for that reason, enhanced NO concentrations due to the return commuting traffic (16:00–19:00) could not be observed.

When enhanced NO concentrations from the district road arrive at any position of the forest edge, the actual surface layer flow will transport the NO from there to the measurement site. This will lead, particularly for NO, to the generation of chemically induced vertical concentration gradients. The wind speed at the forest floor is approximately one order of magnitude lower than above the canopy. This, in turn, allows a tenfold longer time for O_3 to react with NO at the forest floor. The reaction product NO_2, however, will be photolyzed back to NO above the canopy, while in the shadow at the forest floor this reaction is at least strongly suppressed. Both effects lead at the measurement site, finally, to noticeable differences of NO concentrations between above canopy and forest floor. A clear example is shown in the upper panel of Fig. 15, where

a vertical NO gradient (between 31.5 m and 0.9 m a.gr.) of ≥0.3 ppb was observed during 08:00–10:00 (1 July 2008).

Since in the presence of strong horizontal advection and low stationarity of concentrations the interpretation of measured fluxes and/or vertical gradients in terms of turbulent exchange is generally not meaningful, we omitted all NO, NO_2, and O_3 data measured between 06:00 and 12:00 CET from our analysis in Sects. 3.5.2, 3.5.3, and 3.6.2.

3.5 Trace gas fluxes

3.5.1 Time series

Trace gas fluxes which have been measured by eddy covariance technique are shown in Fig. 17 (IOP-1: left panels, a–c; IOP-2: right panels, a–e). They comprise fluxes of water vapor (F_{H_2O}), carbon dioxide (F_{CO_2}), ozone (F_{O_3}), nitrogen dioxide (F_{NO_2}), nitric oxide (F_{NO}), and the composites $F_{O_x} = F_{O_3} + F_{NO_2}$ and $F_{NO_x} = F_{NO} + F_{NO_2}$. During the selected fair-weather days, F_{H_2O} clearly followed diel variations of available energy and H_2O gradients; it was close to zero during night, and up to 200 W m^{-2} flux during day (Fig. 17a). Classic daily variations were found for F_{CO_2}, featuring negative fluxes during daytime (CO_2 uptake by vegetation) and positive (respiration) fluxes during night (Fig. 17 b). As expected, F_{O_3} reflected during both IOPs the well-known O_3 deposition to forest vegetation and ground (Fig. 16c, black symbols), and F_{O_x} followed closely that of F_{O_3} (Fig. 17 c, grey symbols) for the reason explained below (see Sect. 3.5.2). In contrast, F_{NO_2} (measured during IOP-2 only) was mostly directed upwards, with large fluxes during most of the daytime and smaller fluxes during night (Fig. 17d, right panel). For NO, however, peaks of downward directed fluxes were determined during the morning hours, whereas F_{NO} was indistinguishable from zero for the rest of the day and also during night-time (Fig. 17e, right panel).

Data gaps in F_{NO} and F_{NO_2} were due to routine calibration. The flux of the chemically conservative composite NO_x showed a very similar pattern to that of F_{NO_2} (Fig. 17d,

right panel, grey symbols), with the exception of those time periods between 06:00 and 12:00 CET, when F_{NO_x} was substantially lower than F_{NO_2} (due to noticeable $F_{NO} < 0$), which in turn is most likely the result of advection induced, positive, strong vertical gradients of NO concentration above the canopy. Otherwise, $F_{NO_2} \approx F_{NO_x}$, because the contribution of F_{NO} to F_{NO_x} is one order of magnitude lower than that of F_{NO_2}. Therefore, both F_{NO_x} and F_{O_x} (the flux of the chemically conservative composite $O_x = O_3 + NO_2$), and also the respective concentration differences, will not further be considered for the analysis of fluxes and concentration gradients vs. coupling stages (see Sects. 3.4.2 and 3.5.2).

During IOP-2, in the afternoon (12:00–18:00), turbulent NO_2 fluxes measured by eddy-covariance technique at 31.5 m (a.gr.) ranged between + 0.5 and $+\sim$1.8 nmol m^{-2} s^{-1}, i.e. the *Waldstein-Weidenbrunnen* spruce forest appeared as a significant NO_2 source during this time period. Without loss of generality, we may consider this flux just as a net NO_2 flux, namely as the result of a downward directed deposition flux (NO_2 uptake by spruce needles) and an upward directed flux (due to complete oxidation ($NO + O_3 \rightarrow NO_2 + O$) of the NO, which is biogenically emitted from forest soil). Ignoring potential (small) emission of NO_2 from spruce needles (Lerdau et al., 2000) and estimating the NO_2 deposition flux to approx. −0.2 nmol m^{-2} s^{-1} (cf. Breuninger et al., 2011), the corresponding biogenic NO flux from the forest soil should then range between +0.3 and +1.6 nmol m^{-2} s^{-1}. From the results of Bargsten et al. (2010), where soil samples of the *Waldstein-Weidenbrunnen* site were quantified for their net potential NO soil emission, maximum soil NO emissions of +1.7 nmol m^{-2} s^{-1} were estimated for the conditions of IOP-2.

The fluxes of $F_{NH_4^+,tot}$ and $F_{NO_3^-,tot}$ are shown in Fig. 17 (left panels, d and e) and were mostly directed downward to the forest canopy with pronounced diel variations. Wolff et al. (2010b) provide a detailed discussion about the magnitude of $F_{NH_4^+,tot}$ and $F_{NO_3^-,tot}$ with respect to comparable previous studies reported so far. Turbulent time scales (τ_{turb}, Eq. (2)) are also shown in Fig. 17 (panels f); they remained mostly below 50 s during both IOPs.

For reasons given above (Sect. 3.4) those values have been removed from all those data sets of measured fluxes (as well as concentration differences, time scales and Damköhler numbers), which were obtained between 06:00–12:00 CET every day. The remaining data have been classified two-fold: (a) by day- and night-time (defined by time of sunrise and sunset, and (b) by corresponding coupling regimes Dc/Wa, Ds, Cs/C, and then summarized into box-and-whisker plots.

3.5.2 Influence of the coupling situations

All measured fluxes (as well as concentration differences, time scales and Damköhler numbers) have been classified two-fold, (a) by day- and night-time (defined by time of sunrise and sunset, and (b) by corresponding coupling regimes Dc/Wa, Ds, Cs/C, and then summarized into box-and-whisker plots. Figure 18 shows the results of classification (according to Wa/Dc, Ds, Cs/C coupling stages) of turbulent fluxes of water vapor (F_{H_2O}), carbon dioxide (F_{CO_2}), ozone (F_{O_3}), nitrogen dioxide (F_{NO_2}), nitric oxide (F_{NO}), total ammonium ($F_{NH_4+,tot}$), and total nitrate ($F_{NO_3-,tot}$). It has to be kept in mind, that daytime temperature of the air (T_{air}) and relative humidity (rH) showed relatively similar medians and dispersion for the three different coupling regimes. In contrast, daytime median and dispersion of global radiation data (Rg) were much lower during the coupling regime Wa/Dc as compared to the decoupled subcanopy and fully coupled stages, because of the low total number of data and the occurrence of daytime Wa/Dc stages in early morning or late afternoon hours. As expected, night-time values of T_{air}, were lower, and night-time rH were higher than daytime data, and global radiation was zero. Hence, a direct comparison of fluxes (and later concentration differences) for the three coupling stages was only possible at night, or between the Ds and Cs/C stage, as these major driving variables showed similar distributions over the investigated time periods. Daytime fluxes of F_{H_2O}, F_{CO_2}, F_{O_3}, F_{NO_2}, F_{NO}, $F_{NH_4+,tot}$, and $F_{NO_3-,tot}$ replicate the pattern described for global radiation, with less available energy during the Wa/Dc stage compared to Ds and Cs/c stages. As a consequence, upward directed fluxes (F_{H_2O}, F_{NO_2}) are smaller during Wa/Dc, and downward directed fluxes (F_{CO_2}, F_{O_3}, F_{NO},

$F_{NH_4+,tot}$, $F_{NO_3-,tot}$) are larger during Wa/Dc. While F_{H_2O} during night was close to zero and showed small dispersions for all coupling stages and both IOP's (Fig. 18a), F_{CO_2} was positive for both IOPs during night (Fig. 18b). However, when comparing fluxes of different coupling stages, they repeated the pattern of air temperature only in the summer period (IOP-2): lowest medians in Wa/Dc were associated with lowest air temperatures (Fig. 17b, right panel). F_{O_3} during night was more negative in the fall period than in the summer period (Fig. 18c), even though air temperatures were higher (by approx. 4 K) and relative humidity was lower (by approx. 12 %). During both IOPs, night-time F_{O_3} were approx. 50 % lower than daytime O_3 fluxes, which is due to stomata closing during night. However, $F_{O_3} \neq 0$ during night points to a strong non-stomatal component of O_3 uptake, as extensively described by Fowler et al. (2001). F_{NO_2} (measurements during IOP-2 only) showed small fluxes during night (Fig. 18d, right panel). Here, the median during Wa/Dc was lower than those during Ds and Cs/C regimes. However, F_{NO_2} was always significantly > 0, indicating the strong (chemically induced) NO_2 source within the canopy (s. Sect. 3.4.1). During Ds and Cs/C conditions, F_{NO_2} exceeded that NO_2 flux where coupling was (very) low by a factor of approx. 10. This strongly points to the fact that deep canopy mixing is necessary to export the soil emitted NO from the forest floor into the above canopy surface layer (oxidized by O_3 to NO_2 in the first half meter above the forest floor, cf. Fig. 15, top panel).

For NO, night-time fluxes were indistinguishable from zero (Fig. 18e, right panel) and daytime NO fluxes were always negative. During night, zero NO fluxes are due to stomata closure and due to the fact that the solubility of NO is extremely low, and consequently NO hardly deposits to any vegetation elements. Small – but downward directed – NO fluxes during day are most likely resulting from the fact that in the middle of the forest canopy, usually the minimum of the vertical NO distribution is observed (cf. Fig. 15, top panel). This is due to long residence times which favor the nearly complete reaction with O_3 (being 10–100 times higher in concentration than NO). The NO flux then simply follows the NO concentration gradient between above and mid-canopy levels. Both $F_{NH_4+,tot}$ and $F_{NO_3-,tot}$, which have only been measured during

IOP-1 (Fig. 18d and e, left panels) showed small negative values, again with medians during Wa/Dc closer to zero than those during Ds and Cs/C regimes.

3.5.3 The Damköhler number

Turbulent and chemical time scales, as well as Damköhler numbers, have been determined for the above – canopy layer only and all data obtained between 06:00–12:00 have not been considered (s. Sect. 3.4). During daytime, turbulent time scales (τ_{turb}) showed a distinctive pattern of higher medians for the decoupled conditions (Wa/Dc), when comparing different coupling stages (Fig. 19a, b). During night time a similar pattern of higher medians during Wa/Dc conditions can be found (limited by availability of data in certain classes). During IOP-1 and IOP-2, τ_{turb} was longer at night than at day for partly and fully coupled conditions. Chemical time scales (τ_{chem}), however, were fairly constant when comparing different coupling stages separately for day or night-time (Fig. 19 c, d), yet slightly longer at night. When comparing the fall period (IOP-1, Fig. 19c) with the summer period (IOP-2, Fig. 19d), interquartile ranges of τ_{chem} were wider during fall, and τ_{chem} was also longer than during the summer period. Given the relatively constant behavior of τ_{chem}, corresponding Damköhler numbers ($DA = \tau_{turb}/\tau_{chem}$, Fig. 19e, f) reflect the daytime pattern already described for τ_{turb}, with higher medians for decoupled conditions (Wa/Dc). During night-time, medians are still highest for Wa/Dc stages, but dispersion is widest for the Cs/C stages of the summer period. Only during partly or fully coupled summer daytime conditions does part of the interquartile range of Damköhler numbers fall below $DA < 0.1$ (i.e. where reactive trace gases may also be treated as "passive tracers"). Damköhler numbers (Eq. 1), given in Fig. 17g, reflected this pattern, because chemical time scales were relatively constant during the time of our observations (data not shown).

Not surprising is that the turbulent time scales and Damköhler numbers for the coupling stages Ds and Cs/C are nearly identical. Both are determined above the canopy under coupled situation but in the case of Ds the forest floor is, of course, decoupled.

Further research is necessary to investigate whether the use of the turbulent time

scale derived by the gradient approach (Mayer et al., 2011) is the appropriate method in cases when coherent structures dominate the flux (see Sect. 3.2). Therefore, coherent structures should also be detected below 10 s, which is the lowest indicated duration for coherent structures with software used in this paper (Thomas and Foken, 2005). Consequently their duration time and the vertical scale of the structure should be used as the turbulent time scale for the Damköhler number. With such an approach Damköhler numbers may even be significantly below 0.1.

3.6 Above-below canopy concentration differences

We have not pursued determination of in-canopy fluxes according to the classical gradient approach simply for the fact that, particularly in the case of the strong influence of coherent structures, so-called "counter gradients" of meteorological quantities and concentrations may exist throughout the canopy. Therefore, we confined ourselves to typical concentration differences between the trunk space and the top of the canopy. For that, we selected the measurement heights of 24 m (immediately above the canopy) and 1 m (above the forest floor). The latter is, for reactive trace gases, no longer influenced by the strong concentration gradients within the first tens of centimeters above the forest floor (see Fig. 15). For the investigation of vertical gradients (Sect. 3.6.2) all data obtained between 06:00–12:00 have not been considered (see Sect. 3.4).

3.6.1 Time series

During both IOPs, H_2O concentration differences ($\Delta[H_2O] = [H_2O]_{24m} - [H_2O]_{0.9m}$) between the 24 m (canopy top) and 0.9 m (above understory) levels were for most of the daytime negative, and positive during summertime nights, confirming that we have observed well-known fair weather in-canopy gradients with moister conditions below the canopy compared to those above during day, and opposite gradients during night (Fig. 20a). Most of the time, $\Delta[CO_2] = [CO_2]_{24m} - [CO_2]_{0.9m}$ was negative, however,

during daytime it was close to zero; highest CO_2 concentrations were found close to the forest floor at night (Fig. 20b). As expected, $\Delta[O_3] = [O_3]_{24m} - [O_3]_{0.9m}$ was positive during both IOPs, as well as during respective day- and night-times, reflecting the well-known O_3 deposition to ground and vegetation (Fig. 20 c, black symbols). During the fall period (IOP-1), $\Delta[NO_2] = [NO_2]_{24m} - [NO_2]_{0.9m}$ exhibits a small diurnal course (negative during daytime, positive or close to zero during night, Fig. 19d, left panel, black symbols); during most of the summer period (IOP-2), $\Delta[NO_2]$ was clearly negative (see Fig. 20d, right panel, black symbols), once again indicating the already mentioned strong source of NO_2 within the canopy. Gradients of NO_x (=NO_2 + NO) between 24 m and 0.9 m (Fig. 20d, grey symbols) show patterns very similar to those of NO_2, and gradients of O_x (=O_3 + NO_2, Fig. 20c, grey symbols) follow closely those of O_3. The latter is due to O_3 concentrations being one order of magnitude larger than NO_2 during the investigated time periods. Since the forest soil acts as a biogenic source of NO, $\Delta[NO] = [NO]_{24m} - [NO]_{0.9m}$ has actually been expected to be negative (and presumably small). However, positive NO gradients, particularly in the morning hours (06:00–12:00 CET), confirm the advective impact of traffic related NO sources (see Sect. 4.4), especially during IOP-1 (Fig. 20e, left panel), but still visible in IOP-2, too (Fig. 20e, right panel). Only for IOP-1 were gradients of HONO ($\Delta[HONO] = [HONO]_{24m} - [HONO]_{0.9m}$) available (Sörgel et al., 2011). During many of the daytime hours, Δ[HONO] was negative or close to zero, but positive during much of the night (Fig. 20f).

3.6.2 Influence of the coupling situations

For the following analysis, all data sets of measured concentration differences which have been obtained between 06:00–12:00 CET every day have been removed (see Sect. 4.3). During IOP-1, medians and interquartile ranges of H_2O concentration differences ($\Delta[H_2O] = [H_2O]_{24m}$ - $[H_2O]_{0.9m}$) between the 24 m and 0.9 m levels were always negative, indicating moister conditions below the canopy. During IOP-2, night-time

medians were positive, indicating drier below-canopy conditions compared to those above, whereas during the day mostly opposite gradients were observed (Fig. 21a).

For $\Delta[CO_2] = [CO_2]_{24} - [CO_2]_{0.9m}$, medians and interquartile ranges were negative but were, however, closer to zero during the day than during night (Fig. 21b). During daytime Wa/Dc regimes these negative CO_2 gradients were largest, again possibly due Wa/Dc stages close to night-time, with more pronounced CO_2 gradients between above and below canopy. Medians and inter-quartile ranges of $\Delta[O_3]$ were positive for both periods, day- and night-time, and all coupling stages (Fig. 21c). However, during both IOPs larger $\Delta[O_3]$'s were observed at night (medians >12 ppb) as compared to daytime (medians <12 ppb). In the fall period (IOP-1), $\Delta [NO_2] = [NO_2]_{24} - [NO_2]_{0.9m}$ was negative during daytime for the Ds and Cs/C regimes, and positive or close to zero otherwise (Fig. 21d, left panel); during IOP-2 (summer) medians and inter-quartile ranges were clearly negative, with medians slightly more negative (up to −1.3 ppb) and larger interquartile ranges at night (Fig. 21d, right panel). Small negative medians of Δ[NO] were observed for most of the summer period (IOP-2) and during fall (IOP-1) at night-time hours (Fig. 21e). During hours where Ds and Cs/C prevailed, $\Delta [HONO] = [HONO]_{24m} - [HONO]_{0.9m}$ was negative during the daytime hours, and positive during much of the night (Fig. 21f). Under Wa/Dc regimes, medians of Δ[HONO] change sign (day: negative, night: positive), but also show much wider dispersion as indicated by the large inter-quartile range.

Any trial to synthesize Figs. 17 and 21 based on the common flux/gradient relationship $F = -v_{ex} [m(z_2) - m(z_1)]$, for $z_2 > z_1$ are flawed because fluxes F were measured in 32 m, while concentration differences Δm were evaluated between 24 and 0.9 m. Proportionality between the data shown in Fig. 17 (fluxes) and 21 (concentration differences) is therefore not expected. This may sound trivial at first glance, but has rather interesting implications. Comparing Figs. 17 and 21, it is very remarkable that during IOP-1 and IOP-2 the signs of Δm and F for the examined scalars (H_2O, CO_2, O_3, NO_2, and NO) are always compatible under night-time conditions, and nearly always correspond under daytime conditions. That is, negative Δm concur with positive F, and

positive Δm concur with positive F.

However there are two exceptions: negative daytime F_{NO} coincide with negative Δ[NO], and negative daytime F_{CO_2} coincide with negative $\Delta[CO_2]$, with the exception of Wa/Ds stages in IOP-2 (7 values only). What distinguishes daytime CO_2 and NO from the other scalars and from night-time conditions? The answer lies within the "control volume" (i.e. between $z = 0$ m and $z = 32$ m) for a flux measured at $z = 32$ m. Whereas for the sign-conforming cases (night-time conditions and daytime H_2O, O_3, and NO_2) the control volume contains either sources or sinks, for the non-conform scalars (daytime CO_2 and NO) the control volume contains both sources as well as sinks for the respective scalar.

For daytime CO_2, the control volume contains CO_2 sources from soil, trunk and leaf respiration and the even stronger CO_2 sink, i.e. the assimilation by green leaves in understory and canopy. Hence, the mixture of biological sources and sinks within the control volume distorts the conformity between flux and concentration differences. This is completely different during the night, where the CO_2 sink term "assimilation" is missing, only source terms remain, and signs of flux and $\Delta[CO_2]$ are consistent again.

Now, for daytime NO, which is biogenically formed in the soil and emitted from the soil surface to the forest atmosphere, there are no known biological sinks in the control volume. However, most of the emitted NO is oxidized by ozone to NO_2 in the first few tenths of a meter above the forest floor, and a part obviously also still above the first meter. The typical "back reaction", the photolysis of NO_2 to O_3 and NO, is suppressed, since it is comparatively dark below/within the canopy or in the understory. Most of the NO_2 (the former NO) can leave the control volume at $z = 32$ m, because the uptake by the needles is much lower than for O_3 (Breuninger et al., 2011; Geßler et al., 2002). Hence, in the case of NO, the mixture of mainly biological sources and mainly chemical sinks within the control volume is responsible for the non-conformity between flux and concentration differences.

In summary, the attempted – rather qualitative – synopsis of Figs. 17 and 21 made evident a common problem of non-reactive as well as reactive trace gases, namely that a mixture of source and sink terms in the control volume of a flux requires careful assessment of primary sinks and sources, turbulence, and photochemical interactions. Corresponding questions are the subject of ongoing analyses.

Regarding the HONO mixing ratio, differences for Ds and Cs/C regimes are very similar at daytime (slightly negative or close to zero), which can be attributed to the photolytic sink above the forest and heterogeneous formation at the forest floor in the late afternoon. At night time no clear result is possible due to the very limited number of measurements. Sörgel et al. (2011) concluded that differences in source and sink processes in and above the forest canopy became obvious only for the decoupled situations (Wa, Dc, Ds). Otherwise mixing ratio differences were close to zero. The positive values during night could partly be attributed to advection of HONO rich air above the canopy which only partly penetrated the canopy.

A more quantitative analysis of fluxes (or concentration differences) with respect to the coupling stages is, on the one hand, limited by the small number of data points within some of the coupling stages (daytime Wa/Dc during IOP-1 and IOP-2, and night-time Ds during IOP-1). On the other hand, and even more importantly, coupling stages are subject to a typical diurnal and annual variation (see Fig. 12), and therefore superimposed with meteorological differences between the coupling stage categories (see Sect. 3.5.2). Differences in the magnitude of fluxes between the coupling stage classes are therefore mainly due to differences in available energy, atmospheric demand or available soil water (in the case of F_{H_2O}), and only partially influenced by the coupling stage itself. Similarly, the magnitudes of F_{CO_2} (or F_{O_3}) may be modulated by the associated coupling stages, but certainly are driven by radiation, temperature and humidity, which affect stomatal opening (or chemical conversions) and consequently deposition velocities.

3.7 Modelling of fluxes

For EGER IOP-1 campaign, latent heat exchange was analyzed with the three dimensional microclimate and gas exchange model STANDFLUX (Falge et al., 1997, 2000), and the one dimensional model ACASA (Pyles, 2000; Pyles et al., 2000). Both models were parameterized for the *Waldstein-Weidenbrunnen* site. Parameters common to both models included information on vertical leaf area distribution, and specific sets of physiological parameters for top, middle, and bottom canopy leaf gas exchange. STANDFLUX employed, in addition, horizontal leaf area distribution, tree positions and tree sizes. Further information on model theory and setup is found in Staudt et al. (2011). Latent heat exchange is modelled as the energy equivalent of the sum of evaporation from interception pools and upmost soil and litter layer, and tree and understory transpiration.

Prerequisite of comparisons between measured and modeled energy fluxes is a closed energy balance (Falge et al., 2005), because physical models are based on energy balance closure. In former studies, a value of 77 % (Aubinet et al., 2000; Foken, 2008a) was found according to

$$100\,\% - Res = \frac{H + LE + G}{R_\mathrm{n}} \cdot 100\,\% \tag{11}$$

with the net radiation R_n, the sensible heat flux H, the latent heat flux LE, the ground heat flux G, and residual Res. In this study the heat storage was neglected. During both IOPs similar values were found with approx. 80 % for both IOP's (Fig. 22).

Coupling state analysis of measured data and model predictions, based on Thomas and Foken (2007a), complement traditional analyses of data-model comparisons. Three coupling stages are distinguished: wave motion and decoupled canopy (code Wa/Dc, $n = 8$ during daytime, $n = 57$ during night-time), decoupled subcanopy (code Ds, $n = 28$ during daytime, $n = 1$ during night-time), coupled subcanopy by sweeps and entirely coupled (code Cs/C, $n = 68$ during daytime, $n = 18$ during night-time). The use of coupling states demonstrates which turbulence stages are well represented and

which are poorly represented by the model, and thus can serve as a diagnostic tool to improve turbulence parameterizations. By visualizing the data with respect to coupling stages, data-model mismatch at the different stages can be identified (see Fig. 23).

Figure 23 shows that for the daytime decoupled cases (Wa/Dc), both models largely overestimated eddy-covariance measurements, probably resulting from the difficulties in performing eddy-covariance measurements under decoupled conditions. During daytime, STANDFLUX underestimates the measured evapotranspiration, especially for the Cs/C stage (Fig. 23a), when comparing the model results to the eddy covariance data from the turbulence tower at 36 m (Staudt et al., 2011). The performance of STANDFLUX improves when compared against eddy covariance data from the main tower at 32 m (data not shown), because the eddy covariance fluxes measured at the main tower are lower than those measured at the turbulence tower ($LE_{32\mathrm{m}} = 0.92\ LE_{36\mathrm{m}} - 8.8$, $r^2 = 0.88$, for 20–24 Septebmer 2007, and quality flags 1–6), potentially because the two towers sample different footprints. ACASA gave slightly better results compared to the measured evapotranspiration at Ds, and Cs/C stage (Fig. 23b). However, ACASA underestimates canopy transpiration (Staudt et al., 2011); an overestimation of evapotranspiration implies therefore an overestimation of the evaporation sources (soil and interception pool) by the model. For night-time conditions, both models underestimated eddy-covariance measurements during all coupling stages. Reasons for this underestimation might either originate in the models or the eddy-covariance measurements which might be underestimates themselves due to the lack of energy balance closure, exacerbating the underestimation of the models even more. Then again, the eddy-covariance estimates might be overestimating the uniform forest below the tower due to the contribution of clearings to the flux footprint. These clearings were found to act as a source of moisture and thus increase eddy-covariance estimates. The reasons for the modeled underestimation of eddy-covariance transpiration measurements are different for the two models ACASA and STANDFLUX. Ecosystem evapotranspiration modeled with the ACASA model agreed better with eddy-covariance measurements (Fig. 23b), but partly for the wrong reason: an overestimation of soil and

understory evapotranspiration with a constant offset of about 10 W m^{-2}, compensated the modeled canopy transpiration which was too low. In contrast, the STANDFLUX model underestimated both, canopy transpiration and soil and understory evapotranspiration. However, it should be noted that, even though relative errors of the models were large, absolute errors were only 8 W m^{-2} for ACASA and 10 W m^{-2} for STANDFLUX during decoupled conditions, and 15 W m^{-2} for both models for coupled conditions.

High variances are expected because the dynamic footprint always adds to the flux variance at halfhourly time scales, that is, the eddy covariance method does not sample the same patch all the time, whereas the model setup is static. In addition, the relative errors might show larger variances, because the models do not account for sweeps and ejections or for the conditions of the W stage, where neither the assumptions for the model nor for eddy covariance theory are fulfilled. In the stable canopy space stimulation of gravity waves occurs at times (Cava et al., 2004; Lee et al., 1997). Under certain conditions, such waves become nonlinear and lead to ejections from the canopy (Fitzjarrald and Moore, 1990). Because of difficulties in resolving the Reynolds mean, effects of such singular events may be improperly calculated in a halfhourly eddy flux record.

4 Conclusions and outlook

It was the aim of this study (i) to introduce the research project EGER (ExchanGE processes in mountainous Regions), (ii) to present an overview of its conceptual and instrumental design, (iii) to describe the applied methods and multi-scale methodologies, (iv) to investigate site-specific meteorological and micrometeorological conditions (i.e. forest roughness layer, coupling between surface layer and canopy, influence of boundary layer features), and (v) to present first results of above canopy exchange fluxes and concentration differences (above canopy forest floor) of non-reactive and reactive trace gases. The main results and findings are concluded as follows:

– For the investigation of the in- and above-canopy exchange of energy, non-reactive and reactive trace gases, the consistent application of the scale concept (Fig. 7) is necessary, since the underlying soil, biological, chemical and (turbulent) transport processes form a complex multi-scale problem.

– While the individual processes widely overlap in the temporal domain, there is a larger (chemical) or smaller (soil, biological) separation from the turbulent processes regarding the spatial domain. Since for the exchange over tall vegetation (forests) the concept of a flux through an interface has to be replaced by a flux through a volume element, not only 3-D advection became a substantial problem. Volume averaging, necessary to bridge the spatial scale gap between chemical and turbulent processes, is immediately confronted with the reactivity of trace gases (e.g. is the (turbulent) transport through the canopy fast enough to allow soil/plant emitted reactive traces gases to reach the surface layer unchanged?). For the surface layer above the canopy, the ratio of the turbulent time scale over the characteristic chemical time scale, the Damköhler number, seems to be the suitable measure to distinguish trace gases between “passive tracers” and those compounds which will change their concentration significantly during turbulent transport.

– According to Fig. 7, coherent structures do not always follow the typical scaling system and this might increase turbulent mixing (Mahrt, 2010), which would consequently reduce the influence of fast chemical reactions to measured fluxes and concentration differences. First analysis of EGER data sets has already shown that the coupling concept (Thomas and Foken, 2007a) is without doubt a new and substantial tool for the interpretation of above-canopy fluxes and concentration differences (above-canopy versus forest floor). But it seems meaningful that the more point-related approach of the turbulent time scale (necessary for the calculation of the Damköhler number above the canopy) should be replaced by the spatio-temporal scale of coherent structures, which is based on the coupling

concept. At least, this is definitely necessary when the contribution of coherent structures to vertical transport processes dominates (night time, see Figs. 18, 19 and 21).

– It was important to complete the experimental EGER studies by boundary-layer profiling measurements, because boundary-layer phenomena also influence transport processes at the site scale. One of the most investigated phenomena in this respect is that of low-level jets, which may re-distribute vertical concentration profiles (s. Fig. 15) and increase surface fluxes due to strong vertical shear. Similar effects are caused by gravity waves. However, both phenomena are very much related to site- specific conditions.

– The analysis of the coherent structures and the coupling can be applied to an even wider range than shown above. The method of the analysis of coherent structures even offers the selection of sweeps and ejections in and above the canopy. Serafimovich et al. (2011) have shown that coupling is not only a vertical exchange effect but also a horizontal. This horizontal coupling depends substantially on the canopy structure, which may be represented by subcanopy density and the PAI. Therefore a careful analysis of both quantities is essential. This was applied by Siebicke (2011) to give a more general explanation of the night-time in-canopy CO_2-advection problem.

– By comparison the sign of fluxes and gradients, initially only for water vapor and carbon dioxide, the fluxes show the expected diurnal cycle and are widely similar for all days. In contrast to this the gradients only follow these diurnal cycles for some selected periods and show an irregular pattern. This is a strong indication that the concentration measurements near the forest floor are decoupled from the flux and concentration measurements above the canopy. Because the sign of the flux often disagrees with the direction of the gradient, typical counter gradient fluxes occur (Denmead and Bradley, 1985). Further analysis of such situations

needs indicators for a deeper analysis other than the forcing parameters wind and radiation.

– The aerodynamic method of using concentration gradients (observed above the canopy) for the determination of turbulent exchange fluxes can be applied to the *Waldstein-Weidenbrunnen* site only within certain limits, simply because the trees are too high to develop a site-specific roughness-sublayer correction. Furthermore, as shown by Ruppert et al. (2006) for temperature, CO_2 and H_2O, the scalar similarity is not fulfilled for all scalars and not in all spectral ranges. Although not shown here, the application of the Modified Bowen-ratio method (Businger, 1986; Müller et al., 1993) to observed above canopy concentration gradients of the NO–NO_2–O_3 triad also failed due to insufficient significance of the (very small) concentration differences. Nevertheless, the analysis of exchange fluxes of the NH_3–HNO_3–NH_4NO_3 triad between the forest canopy and the atmosphere was successful and indicated the importance of dry deposition of total ammonium and total nitrate as an input of reactive nitrogen to the *Waldstein-Weidenbrunnen* ecosystem (Wolff et al., 2010b).

– Within EGER-IOP-2, one of the first eddy covariance data sets (over any ecosystem) was obtained which consists of high resolution measurements of the complete NO-NO_2-O_3 triad. Data have been quality assured by application of the EUROFLUX methodology (Aubinet et al., 2000) and recent updates of the TK2 (latest version: TK3) software (Mauder and Foken, 2004; Mauder et al., 2008; Mauder and Foken, 2011) and delivered significant NO, NO_2 and O_3fluxes over the *Waldstein-Weidenbrunnen* spruce forest. However, a considerable part of flux measurements might be biased by advection of traffic related NO from the nearby district road. Nevertheless, the results confirm the picture of the exchange of the NO–NO_2–O_3triad over tall vegetation, which is to some extent “contrary” to that observed over low vegetation (e.g. Mayer et al., 2011). While over low vegetation, usually upward directed net NO fluxes (due to biogenic NO emission from soil)

and downward directed net fluxes of NO_2 and O_3 (due to stomata uptake) are observed, there are still downward net O_3 fluxes over tall vegetation, but upward net NO_2 fluxes and downward net NO fluxes. Through a modelling study, Jacob and Bakwin (1991) firstly provided an explanation for this behaviour, namely the oxidation of soil emitted NO by O_3 (from aloft) in the low turbulence regime of the trunk space, which was first experimentally confirmed by Meixner et al. (2003) through measurements of net O_3 and NO fluxes above and NO-NO_2-O_3 concentration profiles within and above a Brazilian primary rainforest. As in the dense rainforest, biogenic NO from the forest floor of the *Waldstein-Weidenbrunnen* site is completely oxidized to NO_2, most likely within the first half meter above the forest floor, and escapes in form of NO_2 to the surface layer above the canopy. First quantification of the NO_2 uptake by spruce needles (field measurements, EGER IOP-2) allowed the estimate of the soil related contribution of the net NO_2 flux over the canopy which agrees well with the soil emitted NO flux (estimated from laboratory measurements).

– Classification of the above canopy net NO_2 fluxes with respect to coupling stages revealed 10-fold higher fluxes for fairly and fully coupled conditions (Ds, Cs/C), compared to the de-coupled conditions (Wa/Dc). This is a very clear indication that deep canopy mixing was necessary to export the soil emitted NO from the forest floor into the surface layer above the canopy.

– The diurnal evolution of HONO mixing ratio differences in and above the forest canopy could be well explained by the different source and sink processes (e.g. photolysis, heterogeneous formation and advection) in combination with the coupling regimes (Sörgel et al., 2011). During periods of complete coupling of the forest to the atmosphere (C and Cs), mixing ratio differences were close to zero, despite large differences (factor 10 to 25) in the photolytic sink during daytime. This was less obvious in the beginning of the dry period since HONO values were still influenced by the previous rain period (wet surfaces, low mixing ratio levels).

During night-time, higher values above canopy could be partly explained by advection of HONO rich air, whereas higher values below canopy in the afternoon when the forest was decoupled (mostly Ds and later afternoon Dc and Wa) from the atmosphere pointed to a local source at the forest floor. In summary, the magnitude of the differences in mixing ratios above and below canopy were determined by the amount of vertical mixing, whereas the sign was determined by different source or sink processes.

– Eddy-covariance measurements are, in combination with footprint and data quality analysis, a well established tool for flux investigation, not only above the forest but also – in the case of developed turbulence – within the forest. This was shown not only with the measurements themselves but also in comparison with model results (Staudt et al., 2011).

– Keeping the uncertainties of the measurements in mind, the performance of the one-dimensional ACASA and the three-dimensional STANDFLUX models for water exchange of the forest depends on the time of the day and the coupling conditions. Both models fall short of describing night-time evapotranspiration measurements, yet there is a better performance of the third-order closure model ACASA with an advanced representation of turbulence at night. Regardless of the individual model setup, i.e. three-dimensional versus one-dimensional representation of the stand, both model performances improved considerably during daytime, particularly for coupled and partly coupled situations.

Summarizing the first results of EGER, the combination of a scale (micrometeorological) concept, based on detailed investigations of the structure of atmospheric turbulence, and measurements of reactive and non-reactive trace gases showed interesting and new results which could only be briefly covered in this study. Classification of (i) exchange fluxes observed above the canopy, (ii) turbulent and chemical time scales, and (iii) concentration differences (above-canopy versus forest floor) according to coupling stages, provides a powerful tool for qualitative (and most likely also quantitative)

analysis of exchange processes of non-reactive, and particularly of reactive, trace compounds, and hence allows a better understanding than by interpretation of time series alone. There is certainly more effort and research necessary to make this tool a standard interpretive tool.

Finally, it should be emphasized that the investigation of the surface exchange of reactive trace gases, particularly those which are related to nearby anthropogenic (traffic) sources, could be strongly biased (if not endangered) by horizontal advection of temporally highly variable concentrations. Furthermore, there are different phenomena (LLJ, gravity waves) in the atmospheric boundary layer which might have drastic effects on the vertical distribution of non-reactive and reactive trace compounds and consequently on the observed exchange fluxes. Future field experiments should be designed such that these phenomena could be quantitatively considered, which may have decisive effects on above and in-canopy concentration profiles as well as exchange fluxes.

However, the potential influence of the nearby clear-cut with convection and advection events, and probably a circulation system at times – as suggested as a result of the energy balance closure – between the clear-cut and the forest has not been addressed so far. To investigate these influences a special experiment was realized in June/July 2011 in combination with Large-Eddy Simulations. However there are still issues which need further investigations, such as gradients and fluxes close to the ground. These issues are under investigation. And finally, the large data set also offers the possibility for cooperation with other partners.

Appendix A

In-canopy turbulence structure

The turbulence structure can typically be described with the so-called integral turbulence characteristics (normalized standard deviations), which are nearly constant (Panofsky and Dutton, 1984) or have a small sensitivity to stratification (for an overview

see Foken, 2008b). While the profiles of the mean wind speed above a canopy are strongly affected by the existence of the roughness sublayer (see Sect. 3.1), the effect on integral characteristics is not well investigated and only a few investigations are available (Finnigan, 2000; Raupach et al., 1996). The turbulence characteristics within a forest are spatially heterogeneous and distinct from those associated with the surface boundary layer (Baldocchi and Meyers, 1998). For measurements inside the canopy ($z < h_c$) a parameterization was proposed by Rannik et al. (2003)

$$\frac{\sigma_i}{u_*} = \alpha_i \left\{ \exp\left[-\alpha_i \left(1 - \frac{z}{h_c} \right)^{\beta_i} \right] (1 - \gamma_i) + \gamma_i \right\}$$
$$i = u, v, w; z < h_c \qquad \text{(A1)}$$

and above the canopy constant values were assumed

$$\frac{\sigma_i}{u_*} = \alpha_i$$
$$i = u, v, w; z < h_c \qquad \text{(A2)}$$

The values are given in Table A1. These are based on the measurements shown in Fig. 3.

Acknowledgements. We are grateful for the support by the Bayreuth Center of Ecology and Environmental Research (BayCEER), mainly of G. Müller. Our thanks also go to J. Olesch and J. Sintermann for their support on the field site. We would also like to thank the Karlsruhe Institute of Technology and John Tenhunen (University of Bayreuth) for the support with measuring equipment and Ralph Dlugi, Bernd Huwe, Eberhard Schaller and Franz H. Berger for the intensive discussion during the preparation phase of the project and especially for the development of the scale analysis.

The project was funded by the German Science foundation (DFG) under the contract numbers DFG projects: FO 226/16-1, ME 2100/4-1, ZE 792/4-1 and the Max Planck Society. The continuously running meteorological systems were supported by the Oberfrankenstiftung e.V. under the contract number 01879. Analyses of the wet deposition were made by the Bavarian Environment Agency Augsburg and the chemical soil analysis by the Central Laboratory of BayCEER.

The windprofiler data were kindly made available by the Richard-Aßmann-Observatory of the German Meteorological Service.

References

Amiro, B. D.: Comparison of turbulence statistics within three boreal forest canopies, Boundary-Layer Meteorol., 51, 99–121, 1990.

Ammann, M., Rössler, E., Strekowski, R., and George, C.: Nitrogen dioxide multiphase chemistry: Uptake kinetics on aqueous solutions containing phenolic compounds, Phys. Chem. Chem. Phys., 7, 2513–2518, 2005.

Arya, S. P.: Introduction to Micrometeorology, Academic Press, San Diego, 415 pp., 2001.

Atkinson, R., Baulch, D. L., Cox, R. A., Crowley, J. N., Hampson, R. F., Hynes, R. G., Jenkin, M. E., Rossi, M. J., and Troe, J.: Evaluated kinetic and photochemical data for atmospheric chemistry: Volume I – gas phase reactions of O_x, HO_x, NO_x and SO_x species, Atmos. Chem. Phys., 4, 1461–1738, doi:10.5194/acp-4-1461-2004, 2004.

Aubinet, M.: Eddy covariance CO_2 flux measurements in nocturnal conditions: An analysis of the problem, Ecol. Appl., 18, 1368–1378, 2008.

Aubinet, M., Grelle, A., Ibrom, A., Rannik, Ü., Moncrieff, J., Foken, T., Kowalski, A. S., Martin, P. H., Berbigier, P., Bernhofer, C., Clement, R., Elbers, J., Granier, A., Grünwald, T., Morgenstern, K., Pilegaard, K., Rebmann, C., Snijders, W., Valentini, R., and Vesala, T.: Estimates of the annual net carbon and water exchange of forests: The EUROFLUX methodology, Adv. Ecol. Res., 30, 113–175, 2000.

Aubinet, M., Heinesch, B., and Yernaux, M.: Horizontal and vertical CO_2 advection in a sloping forest, Boundary-Layer Meteorol., 108, 397–417, 2003.

Aubinet, M., Feigenwinter, C., Heinesch, B., Bernhofer, C., Canepa, E., Lindroth, A., Montagnani, L., Rebmann, C., Sedlak, P., and van Gorsel, E.: Direct advection measurements do not help to solve the night-time CO_2 closure problem: Evidence from three different forests, Agric. Forest. Meteorol., 150, 655–664, 2010.

Baldocchi, D. and Meyers, T.: On using eco-physiological, micrometeorological and biogeochemical theory to evaluate carbon dioxide, water vapor and trace gas fluxes over vegetation, Agric. Forest. Meteorol., 90, 1–25, 1998.

Baldocchi, D., Falge, E., H., G. L., Olson, R., Hollinger, D., Running, S., Anthoni, P., Bernhofer,

C., Davis, K., Evans, R., Fuentes, J., Goldstein, A., Katul, G., Law, B., Lee, X. H., Malhi, Y., Meyers, T., Munger, W., Oechel, W., PawU, K. T., Pilegaard, K., Schmid, H. P., Valentini, R., Verma, S., and Vesala, T.: FLUXNET: A new tool to study the temporal and spatial variability of ecosystem-scale carbon dioxide, water vapor, and energy flux densities, B. Am. Meteorol. Soc., 82, 2415–2434, 2001.

Banta, R. M., Newsom, R. K., Lundquist, J. K., Pichugina, Y. L., Coulter, R. L., and Mahrt, L.: Nocturnal low-level jet characteristics over Kansas during Cases-99, Boundary-Layer Meteorol., 105, 221–252, 2002.

Bargsten, A., Falge, E., Pritsch, K., Huwe, B., and Meixner, F. X.: Laboratory measurements of nitric oxide release from forest soil with a thick organic layer under different understory types, Biogeosciences, 7, 1425–1441, doi:10.5194/bg-7-1425-2010, 2010.

Beniston, M.: From turbulence to climate, Springer, Berlin, Heidelberg, 328 pp., 1998.

Berger, M., Dlugi, R., and Foken, T.: Modelling the vegetation atmospheric exchange with transilient model, in: Biogeochemistry of Forested Catchments in a Changing Enivironment, A German Gase Study. Ecological Studies, edited by: Matzner, E., Springer, Berlin, Heidelberg, 177–190, 2004.

Bergström, H. and Högström, U.: Turbulent exchange above a pine forest. II, Organized structures, Boundary-Layer Meteorol., 49, 231–263, 1989.

Blöschl, G. and Sivapalan, M.: Scale issues in hydrological modelling - a review, Hydrol. Process., 9, 251–290, 1995.

Breuninger, C., Oswald, R., Kesselmeier, J., and Meixner, F. X.: The dynamic chamber method: trace gas exchange fluxes (NO, NO_2, O_3) between plants and the atmosphere in the laboratory and in the field, Atmos. Meas. Tech. Discuss., 4, 5183–5274, doi:10.5194/amtd-4-5183-2011, 2011.

Businger, J. A.: Evaluation of the accuracy with which dry deposition can be measured with current micrometeorological techniques, J. Appl. Meteorol., 25, 1100–1124, 1986.

Businger, J. A., Wyngaard, J. C., Izumi, Y., and Bradley, E. F.: Flux-profile relationships in the atmospheric surface layer, J. Atmos. Sci., 28, 181–189, 1971.

Cava, D., Giostra, U., Siqueira, M., and Katul, G.: Organised motion and radiative perturbations in the nocturnal canopy sublayer above an even-aged pine forest, Boundary-Layer Meteorol., 112, 129–157, 2004.

Cellier, P. and Brunet, Y.: Flux-gradient relationships above tall plant canopies, Agric. Forest. Meteorol., 58, 93–117, 1992.

Collatz, G. J., Ball, J. T., Grivet, C., and Berry, J. A.: Regulation of stomatal conductance and transpiration, a physiological model of canopy processes, Agric. Forest. Meteorol., 54, 107–136, 1991.

Collineau, S. and Brunet, Y.: Detection of turbulent coherent motions in a forest canopy. Part II: Time-scales and conditional averages, Boundary-Layer Meteorol., 66, 49–73, 1993a.

Collineau, S. and Brunet, Y.: Detection of turbulent coherent motions in a forest canopy. Part I: Wavelet analysis, Boundary-Layer Meteorol., 65, 357–379, 1993b.

Crescenti, G.: The degradation of Doppler sodar performance due to noise: A review, Atmos. Environ., 32, 1499–1509, 1998.

Damköhler, G.: Der Einfluss der Turbulenz auf die Flammengeschwindigkeit in Gasgemischen, Z. Elektrochem., 46, 601–652, 1940.

Denmead, D. T. and Bradley, E. F.: Flux-gradient relationships in a forest canopy, in: The forest-atmosphere interaction, edited by: Hutchison, B. A. and Hicks, B. B., D. Reidel Publ. Comp., Dordrecht, Boston, London, 421–442, 1985.

Dlugi, R.: Interaction of NO_x and VOC's within vegetation, in: Proceedings EUROTRAC-Symposium 92, edited by: Borrell, P. W., SPB Acad. Publ., The Hague, 682–688, 1993.

Eigenmann, R., Metzger, S., and Foken, T.: Generation of free convection due to changes of the local circulation system, Atmos. Chem. Phys., 9, 8587–8600, doi:10.5194/acp-9-8587-2009, 2009.

Falge, E., Tenhunen, J. D., Ryel, R., Alsheimer, M., and Köstner, B.: Modelling age- and density-related gas exchange of Picea abies canopies of the Fichtelgebirge, Germany, Ann. Sci. For., 57, 229–243, 2000.

Falge, E., Reth, S., Brüggemann, N., Butterbach-Bahl, K., Goldberg, V., Oltchev, A., Schaaf, S., Spindler, G., Stiller, B., Queck, R., Köstner, B., and Bernhofer, C.: Comparison of surface energy exchange models with eddy flux data in forest and grassland ecosystems of Germany, Ecol. Mod., 188, 174–216, 2005.

Falge, E., Ryel, R. J., Alsheimer, M., and Tenhunen, J. D.: Effects on stand structure and physiology on forest gas exchange: A simulation study for Norway spruce., Trees, 11, 436–448, 1997.

Farmer, D. K., Wooldridge, P. J., and Cohen, R. C.: Application of thermal-dissociation laser induced fluorescence (TD-LIF) to measurement of HNO_3, $\sum$alkyl nitrates, $\sum$peroxy nitrates, and NO_2 fluxes using eddy covariance, Atmos. Chem. Phys., 6, 3471–3486, doi:10.5194/acp-6-3471-2006, 2006.

Farquhar, G. D. and von Caemmerer, S.: Modeling photosynthetic response to environmental conditions, in: Encyclopia of plant physiology II, 12b, edited by: Lange, O. L., Nobel, P. S., Osmond, C. B., and Ziegler, H., Springer, Berlin, 1982.

Feigenwinter, C., Bernhofer, C., Eichelmann, U., Heinesch, B., Hertel, M., Janous, D., Kolle, O., Lagergren, F., Lindroth, A., Minerbi, S., Moderow, U., Mölder, M., Montagnani, L., Queck, R., Rebmann, C., Vestin, P., Yernaux, M., Zeri, M., Ziegler, W., and Aubinet, M.: Comparison of horizontal and vertical advective CO_2 fluxes at three forest sites, Agric. Forest. Meteorol., 148, 12–24, 2008.

Finnigan, J.: Turbulence in plant canopies, Ann. Rev. Fluid Mech., 32, 519–571, 2000.

Finnigan, J.: An introduction to flux measurements in diffiult conditions, Ecol. Appl., 18, 1340–1350, 2008.

Fitzjarrald, D. R. and Moore, K. E.: Mechanisms of nocturnal exchange between the rain forest and the atmosphere J. Geophys. Res., 95, 16839–16850, 1990.

Foken, T.: Climate change in the Lehstenbach region, in: Biogeochemistry of Forested Catchments in a Changing Enivironment, A German Gase Study. Ecological Studies, edited by: Matzner, E., Springer, Berlin, Heidelberg, 59–66, 2004.

Foken, T.: 50 years of the Monin-Obukhov similarity theory, Boundary-Layer Meteorol., 119, 431–447, 2006.

Foken, T.: The energy balance closure problem – An overview, Ecolog. Appl., 18, 1351–1367, 2008a.

Foken, T.: Micrometeorology, Springer, Berlin, Heidelberg, 308 pp., 2008b.

Foken, T. and Leclerc, M. Y.: Methods and limitations in validation of footprint models, Agric. Forest. Meteorol., 127, 223–234, 2004.

Foken, T. and Wichura, B.: Tools for quality assessment of surface-based flux measurements, Agric. Forest. Meteorol., 78, 83–105, 1996.

Foken, T., Göckede, M., Mauder, M., Mahrt, L., Amiro, B. D., and Munger, J. W.: Post-field data quality control, in: Handbook of Micrometeorology: A Guide for Surface Flux Measurement and Analysis, edited by: Lee, X., Massman, W. J., and Law, B., Kluwer, Dordrecht, 181–208, 2004.

Forkel, R., Klemm, O., Graus, M., Rappenglück, B., Stockwell, W. R., Grabmer, W., Held, A., Hansel, A., and Steinbrecher, R.: Trace gas exchange and gas phase chemistry in a Norway spruce forest: A study with a coupled 1-dimensional canopy atmospheric chemistry emission model, Atmos. Environm., 40, Suppl. 1, 28–42, 2006.

Fowler, D., Flechard, C., Cape, J. N., Storeton-West, R., and Coyle, M.: Measurements of ozone deposition to vegetation quantifying the flux, the stomatal and non-stomatal components, Water, Air and Soil Pollution, 130, 63–74, 2001.
Frankenberger, E.: Untersuchungen über den Vertikalaustausch in den unteren Dekametern der Atmosphäre, Ann. Meteorol., 4, 358–374, 1951.
Ganzeveld, L. N., Lelieveld, J., Dentener, F. J., Krol, M. C., Bowman, A. J., and Roelofs, G. J.: Global soilbiogenic emissions and the role of canopy processes, J. Geophys. Res., 107, 4298, doi:10.1029/2001JD001289, 2002.
Garratt, J. R.: Flux profile relations above tall vegetation, Q. J. Roy. Meteorol. Soc., 104, 199–211, 1978.
Garratt, J. R.: Surface influence upon vertical profiles in the atmospheric near surface layer, Q. J. Roy. Meteorol. Soc., 106, 803–819, 1980.
Garratt, J. R.: The atmospheric boundary layer, Cambridge University Press, Cambridge, 316 pp., 1992.
Gerstberger, P., Foken, T., and Kalbitz, K.: The Lehstenbach and Steinkreuz chatchments in NE Bavaria, Germany, in: Biogeochemistry of Forested Catchments in a Changing Enivironment, A German Gase Study. Ecological Studies, edited by: Matzner, E., Springer, Heidelberg, 15–41, 2004.
Geßler, A., Rienks, M., and Rennenberg, H.: Stomatal uptake and cuticular adsorption contribute to dry deposition of NH3 and NO_2 to needles of adult spruce (Picea abies) trees, New Phytologist, 156, 179–194, 2002.
Göckede, M., Rebmann, C., and Foken, T.: A combination of quality assessment tools for eddy covariance measurements with footprint modelling for the characterisation of complex sites, Agric. Forest. Meteorol., 127, 175–188, 2004.
Göckede, M., Markkanen, T., Hasager, C. B., and Foken, T.: Update of a footprint-based approach for the characterisation of complex measuring sites, Boundary-Layer Meteorol., 118, 635–655, 2006.
Göckede, M., Foken, T., Aubinet, M., Aurela, M., Banza, J., Bernhofer, C., Bonnefond, J. M., Brunet, Y., Carrara, A., Clement, R., Dellwik, E., Elbers, J., Eugster, W., Fuhrer, J., Granier, A., Grünwald, T., Heinesch, B., Janssens, I. A., Knohl, A., Koeble, R., Laurila, T., Longdoz, B., Manca, G., Marek, M., Markkanen, T., Mateus, J., Matteucci, G., Mauder, M., Migliavacca, M., Minerbi, S., Moncrieff, J., Montagnani, L., Moors, E., Ourcival, J.-M., Papale, D., Pereira, J., Pilegaard, K., Pita, G., Rambal, S., Rebmann, C., Rodrigues, A., Rotenberg,

E., Sanz, M. J., Sedlak, P., Seufert, G., Siebicke, L., Soussana, J. F., Valentini, R., Vesala, T., Verbeeck, H., and Yakir, D.: Quality control of CarboEurope flux data – Part 1: Coupling footprint analyses with flux data quality assessment to evaluate sites in forest ecosystems, Biogeosciences, 5, 433–450, doi:10.5194/bg-5-433-2008, 2008.
Griffith, D. W. T., Leuning, R., Denmead, O. T., and Jamie, I. M.: Air-land exchanges of CO_2, CH_4 and N_2O measured by FTIR spectrometry and micrometeorological techniques, Atmos. Environ., 36, 1833–1842, 2002.
Güsten, H. and Heinrich, G.: On-line measurements of ozone surface fluxes: Part I. Methodology and instrumentation, Atmos. Environ., 30, 897–909, 1996.
Gut, A., Scheibe, M., Rottenberger, S., Rummel, U., Welling, M., Ammann, C., Kirkman, G. A., Kuhn, U., Meixner, F. X., Kesselmeier, J., Lehmann, B. E., Schmidt, W., Müller, E., and Piedade, M. T. F.: Exchange fluxes of NO, NO_2, and O_3 at soil and leaf suraces in an Amazonian rain forest, J. Geophys. Res., 107, 8060, doi:8010.1029/2001JD000654, 2002.
Gutzwiller, L., Arens, F., Baltensperger, U., Gäggler, H. W., and Ammann, M.: Significance of Semivolotile Disel Exhaust Organics for Secondary HONO Formation, Environ. Sci. Technol., 36, 677–682, 2002.
Harman, I. N. and Finnigan, J. J.: A simple unified theory for flow in the canopy and roughness sublayer, Boundary-Layer Meteorol., 123, 339–363, 2007.
Harman, I. N. and Finnigan, J. J.: Scalar concentration profiles in the canopy and roughness sublayer, Boundary-Layer Meteorol., 129, 323–351, 2008.
Heland, J., Kleffmann, J., Kurtenbach, R., and Wiesen, P.: A new instrument to measure gaseous nitrous acid (HONO) in the atmosphere, Environ. Sci. Technol., 35, 3207–3012, 2001.
Hendl, M.: Globale Klimaklassifikation, in: Das Klimasystem der Erde, edited by: Hupfer, P., Akademie-Verlag, Berlin, 218–266, 1991.
Högström, U.: Non-dimensional wind and temperature profiles in the atmospheric surface layer: A re-evaluation, Boundary-Layer Meteorol., 42, 55–78, 1988.
Högström, U.: Review of some basic characteristics of the atmospheric surface layer, Boundary-Layer Meteorol., 78, 215–246, 1996.
Horii, C. P., Munger, J. W., Wofsy, S., Zahniser, M., Nelson, D., and McManus, J. B.: Fluxes of nitrogen oxides over a temperate deciduous forest, J. Geophys. Res., 109, D08305, doi:10.1029/2003JD004326, 2004.
Inclan, M. G., Forkel, R., Dlugi, R., and Stull, R. B.: Application of transilient turbulent theory to

study interactions between the atmospheric boundary layer and forest canopies, Boundary-Layer Meteorol., 79, 315–344, 1996.
Jacob, D. J. and Bakwin, P. S.: Cycling of NO_x in tropical forest canopies, in: Microbial Production and Consumption of Greenhouse Gases: Methane, Nitrogen Oxides and Halomethanes, edited by: Rogers, J. E., and Whitman, W. B., Am. Soc. Microbiol., Washington, 237–253, 1991.
Jacobson, M. Z.: Fundamentals of atmospheric modelling, 2 Edn., Cambridge University Press, Cambridge, 813 pp., 2005.
Jarvis, P. G.: Scaling processes and problems, Plant, Cell Env., 18, 1079–1089, 1995.
Karipot, A., Leclerc, M. Y., Zhang, G., Martin, T., Starr, D., Hollinger, D., McCaughey, H., and Hendrey, G. M.: Nocturnal CO_2 exchange over tall forest canopy associated with intermittent low-level jet activity, Theor. Appl. Climatol., 95, 243–248, 2005.
Karipot, A., Leclerc, M. Y., Zhang, G., Lewin, K. F., Nagy, J., Hendrey, G. R., and Starr, D.: Influence of nocturnal low-level jet on turbulence structure and CO_2 flux measurements over a forest canopy J. Geophys. Res., 113, D10102, doi:10.1029/2007JD009149, 2008.
Katul, G., Kuhn, G., Schieldge, J., and Hsieh, C.-I.: The ejection-sweep character of scalar fluxes in the unstable surface layer, Boundary-Layer Meteorol., 83, 1–26, 1997.
Kleffmann, J.: Daytime sources of nitrous acid (HONO) in the atmospheric aoundary layer, Chem. Phys. Chem., 8, 1137–1144, 2007.
Kleffmann, J., Heland, J., Lörzer, J. C., and Wiesen, P.: A new instrument (LOPAP) for the detection of nitrous acid (HONO), Environm. Sci. Pollution Res., 9, 48–54, 2002.
Kleffmann, J., Gavriloaiei, T., Hofzumahaus, A., Holland, F., Koppmann, R., Rupp, L., Schlosser, R., Siese, M., and Wahner, A.: Daytime formation of nitrous acid: A major source of OH radicals in a forest, Geophys. Res. Lett., 32, L05818, doi:10.1029/2005GL022524, 2005.
Klemm, O., Held, A., Forkel, R., Gasche, R., Kanter, H.-J., Rappenglück, B., Steinbrecher, R., Müller, K., Plewka, A., Cojocariu, C., Kreuzwieser, J., Valverde-Canossa., Schuster, G., Moortgat, G. K., Graus, M., and Hansel, A.: Experiments on forest/atmosphere exchange: Climatology and Fluxes during two summer campaigns in NE Bavaria, Atmos. Environ., 40, Supplement 1, 3–20, 2006.
Lee, X.: On micrometeorological observations of surface-air exchange over tall vegetation, Agric. Forest. Meteorol., 91, 39–49, 1998.
Lee, X., Neumann, H. H., Den Hartog, G., Fuentes, J. D., Black, T. A., Mickle, R. E., Yang,

P. C., and Blanken, P. D.: Observation of gravity waves in a boreal forest, Boundary-Layer Meteorol., 84, 383–398, 1997.
Lenschow, D. H.: Reactive trace species in the boundary layer from a micrometeorological perspective, J. Meteor. Soc. Japan, 60, 472–480, 1982.
Lerdau, M. T., Munger, J. W., and Jacob, D. J.: The NO_2 flux conundrum, Science, 289, 2291–2293, 2000.
Leuning, R. F. M.: Modeling stomatal behavior and photosynthesis of Eucalyptus grandis, Austr. J. Plant Phys., 17, 159–175, 1990.
Liu, H. and Foken, T.: A modified Bowen ratio method to determine sensible and latent heat fluxes, Meteorol. Z., 10, 71–80, 2001.
Lüers, J., Foken, T., Grasse, B., and Döbele, T.: Jahresbericht 2008 zum Förderprojekt 01879, Untersuchung der Veränderung der Konzentration von Luftbeimengungen und Treibhausgasen im hohen Fichtelgebirge, Arbeitsergebn., Univ. Bayreuth, Abt. Mikrometeorol., ISSN 1614-89166, 39, 25 pp., 2009.
Mahrt, L.: Computing turbulent fluxes near the surface: Needed improvements, Agric. Forest. Meteorol., 150, 501–509, 2010.
Mauder, M. and Foken, T.: Documentation and instruction manual of the eddy covariance software package TK2, Arbeitsergebn., Univ. Bayreuth, Abt. Mikrometeorol., ISSN 1614-89166, 26, 42 pp., 2004.
Mauder, M. and Foken, T.: Documentation and instruction manual of the eddy covariance software package TK3, Arbeitsergebn., Univ. Bayreuth, Abt. Mikrometeorol., ISSN 1614-89166, 46, 58 pp., 2011.
Mauder, M., Foken, T., Clement, R., Elbers, J. A., Eugster, W., Grnwald, T., Heusinkveld, B., and Kolle, O.: Quality control of CarboEurope flux data – Part 2: Inter-comparison of eddy-covariance software, Biogeosciences, 5, 451–462, doi:10.5194/bg-5-451-2008, 2008.
Mayer, J. C., Bargsten, A., Rummel, U., Meixner, F. X., and Foken, T.: Distributed Modified Bowen Ratio method for surface layer fluxes of reactive and non-reactive trace gases, Agric. Forest. Meteorol., 151, 655–668, 2011.
Meixner, F. X., Andreae, M. O., van Dijk, S. M., Gut, A., Rummel, U., Scheibe, M., and Welling, M.: Biosphere-atmosphere exchange of reactive trace gases in a primary rainforest ecosystem: studies on interlinking scales, Rep. Ser. Aerosol Sci., 62A, 269–274, 2003.
Meyers, T. P.: A simulation of the canopy microenvironment using higher order closure principles, PhD Thesis, Purdue University, Purdue, 153 pp., 1985.

Meyers, T. P. and Paw U, K. T.: Testing a higher-order closure model for modelling airflow within and above plant canopies, Boundary-Layer Meteorol., 37, 297–311, 1986.
Meyers, T. P. and Paw U, K. T.: Modelling the plant canopy microenvironment with higher-order closure principles, Agric. Forest. Meteorol., 41, 143–163, 1987.
Miller, K. and Rochwarger, M.: On estimates of spectral moments in the presence of colored noise, IEEE Trans. Inf. Theory, 16, 303–308, 1970.
Mölder, M., Grelle, A., Lindroth, A., and Halldin, S.: Flux-profile relationship over a boreal forest – roughness sublayer correction, Agric. Forest. Meteorol., 98–99, 645–648, doi:10.1016/S0168-1923(99)00131-8, 1999.
Moncrieff, J. B., Massheder, J. M., DeBruin, H., Elbers, J., Friborg, T., Heusinkveld, B., Kabat, P., Scott, S., Søgaard, H., and Verhoef, A.: A system to measure surface fluxes of momentum, sensible heat, water vapor and carbon dioxide, J. Hydrol., 188–189, 589–611, doi:10.1016/S0022-1694(96)03194-0, 1997.
Monteith, J. L. and Unsworth, M. H.: Principles of environmental physics, 3rd edition, Elsevier, Academic Press, Amsterdam, Boston, 418 pp., 2008.
Mozurkewich, M.: The dissociation constant of ammonium nitrate and its dependence on temperature, relative humidity and particle size, Atmos. Environ., Part A, General Topics, 27, 261–270, 1993.
Müller, H., Kramm, G., Meixner, F. X., Fowler, D., Dollard, G. J., and Possanzini, M.: Determination of HNO_3 dry deposition by modified Bowen ratio and aerodynamic profile techniques, Tellus, 45B, 346–367, 1993.
Neff, W. and Coulter, R. L.: Acoustic Remote Sensing, in: Probing the atmospheric boundary layer, edited by: Lenschow, D. H., Am. Meteorol. Soc., Boston, 201–239, 1986.
Nenes, A., Pandis, S. N., and Pilinis, C.: ISORROPIA: A new thermodynamic equilibrium model for multiphase multicomponent inorganic aerosols, Aquatic Geochem., 4, 123–152, 1998.
Orlanski, I.: A rational subdivision of scales for atmospheric processes, B. Am. Meteorol. Soc., 56, 527–530, 1975.
Panofsky, H. A. and Dutton, J. A.: Atmospheric Turbulence - Models and methods for engineering applications, John Wiley and Sons, New York, 397 pp., 1984.
Paw U, K. T. and Gao, W.: Application of solutions to non-linear energy budget equations, Agric. Forest. Meteorol., 43, 121–145, 1988.
Paw U, K. T., Baldocchi, D., Meyers, T. P., and Wilson, K. B.: Correction of eddy covariance measurements incorporating both advective effects and density fluxes, Boundary-Layer

Meteorol., 97, 487–511, 2000.
Pryor, S. C., Larsen, S. E., Soerensen, L. L., Barthelmie, R. J., Groenholm, T., Kulmala, M., Launiainen, S., Rannik, U., and Vesala, T.: Particle fluxes over forests: Analyses of flux methods and functional dependencies, J. Geophys. Res., 112, D07205, doi:07210.01029/02006JD008066, 2007.
Pyles, R. D.: The development and testing of the UCD advanced canopy-atmosphere-soil algorithm (ACASA) for use in climate prediction and field studies, University of California, University of California, Davis, 194 pp., 2000.
Pyles, R. D., Weare, B. C., and Paw U, K. T.: The UCD Advanced Canopy-Atmosphere-Soil Algorithm: comparisons with observations from different climate and vegetation regimes, Q. J. Roy. Meteorol. Soc., 126, 2951–2980, 2000.
Rannik, U., Markkanen, T., Raittila, T., Hari, P., and Vesala, T.: Turbulence statistics inside and above forest: Influence on footprint prediction, Boundary-Layer Meteorol., 109, 163–189, 2003.
Raupach, M. R. and Legg, B. J.: The uses and limitations of flux-gradient relationships in micrometeorology, Agricult. Water Managem., 8, 119–131, 1984.
Raupach, M. R. and Thom, A. S.: Turbulence in and above plant canopies, Ann. Rev. Fluid Mech., 13, 97–129, 1981.
Raupach, M. R., Thom, A. S., and Edwards, I.: A wind-tunnel study of turbulent flow close to regularly arrayed rough surface, Boundary-Layer Meteorol., 18, 373–379, 1980.
Raupach, M. R., Finnigan, J. J., and Brunet, Y.: Coherent eddies and turbulence in vegetation canopies: the mixing-layer analogy, Boundary-Layer Meteorol., 78, 351–382, 1996.
Rebmann, C., Anthoni, P., Falge, E., Göckede, M., Mangold, A., Subke, J.-A., Thomas, C., Wichura, B., Schulze, E. D., Tenhunen, J., and Foken, T.: Carbon budget of a spruce forest ecosystem, in: Biogeochemistry of Forested Catchments in a Changing Enivironment, A German Gase Study. Ecological Studies, edited by: Matzner, E., Ecological Studies, Springer, Berlin, Heidelberg, 143–160, 2004.
Rebmann, C., Göckede, M., Foken, T., Aubinet, M., Aurela, M., Berbigier, P., Bernhofer, C., Buchmann, N., Carrara, A., Cescatti, A., Ceulemans, R., Clement, R., Elbers, J., Granier, A., Grünwald, T., Guyon, D., Havránková, K., Heinesch, B., Knohl, A., Laurila, T., Longdoz, B., Marcolla, B., Markkanen, T., Miglietta, F., Moncrieff, H., Montagnani, L., Moors, E., Nardino, M., Ourcvial, J.-M., Rambal, S., Rannik, U., Rotenberg, E., Sedlak, P., Unterhuber, G., Vesala, T., and Yakir, D.: Quality analysis applied on eddy covariance measurements at

complex forest sites using footprint modelling, Theor. Appl. Climat., 80, 121–141, 2005.
Rummel, U., Ammann, C., Gut, A., Meixner, F. X., and Andreae, M. O.: Eddy covariance measurements of nitric oxide flux within an Amazonian rainforest, J. Geophys. Res., 107, 8050, doi:10.1029/2001JD000520, 2002.
Ruppert, J., Thomas, C., and Foken, T.: Scalar similarity for relaxed eddy accumulation methods, Boundary-Layer Meteorol., 120, 39–63, 2006.
Scanlon, T. M. and Albertson, J. D.: Turbulent transport of carbon dioxide and water vapor within a vegetation canopy during unstable conditions: Identification of episodes using wavelet analysis, J. Geophys. Res., D106, 7251–7262, 2001.
Schoonmaker, P. K.: Paleoecological perspectives on ecological scales, in: Ecological Scale, edited by: Peterson, D. L., and Parker, V. T., Columbia University Press, New York, 79–103, 1998.
Seifert, W.: Klimaänderung und (Winter-) Tourismus im Fichtelgebirge - Auswirkungen, Wahrnehmung und Ansatzpunkte zukünftiger touristischer Entwicklung, Fakultät für Biologie, Chemie und Geowissenschaften, Universität Bayreuth, Bayreuth, 206 + XL pp., 2004.
Serafimovich, A., Siebicke, L., Staudt, K., Lüers, J., Biermann, T., Schier, S., Mayer, J.-C., and Foken, T.: ExchanGE processes in mountainous Regions (EGER): Documentation of the Intensive Observation Period (IOP-1), 6 September to 7 October 2007, Arbeitsergebn., Univ. Bayreuth, Abt. Mikrometeorol., ISSN 1614-89166, 36, 145 pp., 2008a.
Serafimovich, A., Siebicke, L., Staudt, K., Lüers, J., Hunner, M., Gerken, T., Schier, S., Biermann, T., Rütz, F., Buttlar, J. v., Riederer, M., Falge, E., Mayer, J.-C., and Foken, T.: ExchanGE processes in mountainous Regions (EGER): Documentation of the Intensive Observation Period (IOP-2) 1 June to 15 July 2008, Arbeitsergebn., Univ. Bayreuth, Abt. Mikrometeorol., ISSN 1614-89166, 37, 180 pp., 2008b.
Serafimovich, A., Thomas, C., and Foken, T.: Vertical and horizontal transport of energy and matter by coherent motions in a tall spruce canopy, Boundary-Layer Meteorol., 140, 429–451, doi:10.1007/s10546-011-19619-z, 2011.
Shaw, R. H.: Secondary wind speed maxima inside plant canopies, J. Appl. Meteorol., 16, 514–521, 1977.
Shaw, R. H., Tavangar, J., and Ward, D. P.: Structure of the Reynolds stress in a canopy layer, J. Climate Appl. Meteorol., 22, 1922–1931, 1983.
Siebicke, L.: Footprint synthesis for the FLUXNET site Waldstein/Weidenbrunnen (DE-Bay) during the EGER experiment, Arbeitsergebn., Univ. Bayreuth, Abt. Mikrometeorol., ISSN

1614-89166, 38, 45 pp, 2008.
Siebicke, L.: Advection at a forest site – an updated approach, PhD Thesis, University of Bayreuth, Bayreuth, 113 pp., 2011.
Simpson, I. J., Thurtell, G. W., Neumann, H. H., Hartog, G. D., and Edwards, G. C.: The validity of similarity theory in the roughness sublayer above forests., Boundary-Layer Meteorol., 87, 69–99, 1998.
Smirnova, T. G., Brown, J. M., and Benjamin, S. G.: Performance of different soil model configurations in simulating ground surface temperature and surface fluxes, Mon. Weather Rev., 125, 1870–1884, 1997.
Smirnova, T. G., Brown, J. M., Benjamin, S. G., and Kim, D.: Parameterization of cold-season processes in the MAPS land-surface scheme, J. Geophys. Res., D105, 4077–4086, 2000.
Sörgel, M., Trebs, I., Serafimovich, A., Moravek, A., Held, A., and Zetzsch, C.: Simultaneous HONO measurements in and above a forest canopy: influence of turbulent exchange on mixing ratio differences, Atmos. Chem. Phys., 11, 841–855, doi:10.5194/acp-11-841-2011, 2011.
Staudt, K. and Foken, T.: Documentation of reference data for the experimental areas of the Bayreuth Centre for Ecology and Environmental Research (BayCEER) at the Waldstein site, Arbeitsergebn., Univ. Bayreuth, Abt. Mikrometeorol., ISSN 1614-89166, 35, 35 pp., 2007.
Staudt, K., Serafimovich, A., Siebicke, L., Pyles, R. D., and Falge, E.: Vertical structure of evapotranspiration at a forest site (a case study), Agric. Forest. Meteorol., 151, 709–729, 2011.
Stelson, A. W. and Seinfeld, J. H.: Relative-humidity and temperature-dependence of the ammonium-nitrate dissociation-constant, Atmos. Environ., 16, 983–992, 1982.
Stockwell, W. R. and Forkel, R.: Ozone and volatile hydrocarbons: isoprene, terpenes, aldehydes, and organic acids, in: Tree Physiology, Vol. 3., Trace Gas Exchange in Forest Ecosystems, edited by: Gasche, R., Papen, H., and Rennenberg, H., Kluwer, Dordrecht, 2570–276, 2002.
Stull, R. B.: An Introduction to Boundary Layer Meteorology, Kluwer Acad. Publ., Dordrecht, Boston, London, 666 pp., 1988.
Su, H.-B., Paw U, K. T., and Shaw, R. H.: Development of a coupled leaf and canopy model for the simulation of plant-atmosphere interactions, J. Appl. Meteorol., 35, 733–748, 1996.
Thomas, C. and Foken, T.: Detection of long-term coherent exchange over spruce forest, Theor. Appl. Clim., 80, 91–104, 2005.

Thomas, C. and Foken, T.: Organised motion in a tall spruce canopy: Temporal scales, structure spacing and terrain effects, Boundary-Layer Meteorol., 122, 123–147, 2007a.
Thomas, C. and Foken, T.: Flux contribution of coherent structures and its implications for the exchange of energy and matter in a tall spruce canopy, Boundary-Layer Meteorol., 123, 317–337, 2007b.
Thomas, C., Mayer, J.-C., Meixner, F. X., and Foken, T.: Analysis of the low-frequency turbulence above tall vegetation using a Doppler sodar, Boundary-Layer Meteorol., 119, 563–587, 2006.
Thomas, C., Martin, J. G., Göckede, M., Siqueira, M. B., Foken, T., Law, B. E., Loescher, H. W., and Katul, G.: Estimating daytime subcanopy respiration from conditional sampling methods applied to multi-scalar high frequency turbulence time series, Agric. Forest. Meteorol., 148, 1210–1229, 2008.
Thomas, R. M., Trebs, I., Otjes, R., Jongejan, P. A. C., Brink, H. T., Phillips, G., Kortner, M., Meixner, F. X., and Nemitz, E.: An automated analyzer to measure aurface-atmosphere exchange fluxes of water soluble inorganic aerosol compounds and reactive trace gases., Environ. Sci. Technol., 43, 1412–1418, doi:10.1021/es8019403, 2009.
Trebs, I., Meixner, F. X., Slanina, J., Otjes, R., Jongejan, P., and Andreae, M. O.: Real-time measurements of ammonia, acidic trace gases and water-soluble inorganic aerosol species at a rural site in the Amazon Basin, Atmos. Chem. Phys., 4, 967–987, doi:10.5194/acp-4-967-2004, 2004.
Verhoef, A., McNaughton, K. G., and Jacobs, A. F. G.: A parameterization of momentum roughness length and displacement height for a wide range of canopy densities, Hydrol. Earth Syst. Sci., 1, 81–91, doi:10.5194/hess-1-81-1997, 1997.
Vilà-Guerau de Arellano, J.: Bridging the gap between atmospheric physics and chemistry in studies of small-scale turbulence, B. Am. Meteorol. Soc., 84, 51–56, 2003.
Vogel, H.-J. and Roth, K.: Moving through scales of flow and transport in soil, J. Hydrol., 272, 95–106, 2003.
Vogel, J. C.: Recycling of carbon in a forest environment, Oecol. Plant, 13, 89–94, 1978.
Wichura, B., Ruppert, J., Delany, A. C., Buchmann, N., and Foken, T.: Structure of carbon dioxide exchange processes above a spruce Forest, in: Biogeochemistry of Forested Catchments in a Changing Enivironment, A German Gase Study. Ecological Studies, edited by: Matzner, E., Ecological Studies, Springer, Berlin, Heidelberg, 161–176, 2004.
Wichura, B.: Untersuchung zum Kohlendioxid-Austausch über einem Fichtenwaldbestand,

Hyperbolic-Relaxed-Eddy-Accumulation Messungen für das stabile Kohlenstoffisotop ^{13}C und Waveletanalysen des turbulenten Kohlendioxid-Austauschs, Bayreuther Forum Ökologie, 114, 297 pp., 2009.
Wilczak, J. M., Oncley, S. P., and Stage, S. A.: Sonic anemometer tilt correction algorithms, Boundary-Layer Meteorol., 99, 127–150, 2001.
Wolff, V., Trebs, I., Ammann, C., and Meixner, F. X.: Aerodynamic gradient measurements of the NH_3-HNO_3-NH_4NO_3 triad using a wet chemical instrument: an analysis of precision requirements and flux errors, Atmos. Meas. Tech., 3, 187–208, doi:10.5194/amt-3-187-2010, 2010a.
Wolff, V., Trebs, I., Foken, T., and Meixner, F. X.: Exchange of reactive nitrogen compounds: concentrations and fluxes of total ammonium and total nitrate above a spruce canopy, Biogeosciences, 7, 1729–1744, doi:10.5194/bg-7-1729-2010, 2010b.
Wulfmeyer, V., Behrendt, A., Kottmeier, C., Corsmeier, U., Barthlott, C., Craig, G., Hagen, M., Althausen, D., Aoshima, F., Arpagaus, M., Bauer, H. S., Bennett, L., Blyth, A., Brandau, C., Champollion, C., Crewell, S., Dick, G., Di Girolamo, P., Dorninger, M., Dufournet, Y., Eigenmann, R., Engelmann, R., Flamant, C., Foken, T., Gorgas, T., Grzeschik, M., Handwerker, J., Hauck, C., Höller, H., Junkermann, W., Kalthoff, N., Kiemle, C., Klink, S., König, M., Krauß, L., Long, C. N., Madonna, F., Mobbs, S., Neininger, B., Pal, S., Peters, G., Pigeon, G., Richard, E., Rotach, M., Russchenberg, H., Schwitalla, T., Smith, V., Steinacker, R., Trentmann, J., Turner, D. D., van Baelen, J., Vogt, S., Volkert, H., T., W., Wernli, H., Wieser, A., and Wirth, M.: The convective and orographically induced precipitation study (COPS): The scientific strategy, the field phase, and research highlights, Q. J. Roy. Meteorol. Soc., 137, 3–30, 2011.
Wyngaard, J. C.: Boundary-Layer Modelling, in: Atmospheric Turbulence and Air Pollution Modelling, edited by: Nieuwstadt, F. T. M. and Van Dop, H., Reidel, Dordrecht, 69–106, 1982.

Table 1. Climate data for *Waldstein-Pflanzgarten* (period 1971–2000, Foken, 2003) and climate trends (Foken, 2004; Seifert, 2004).

Parameter	Climate (1971–2000)	Climate trend
height a.s.l.	765 m	
climate zone *	Dc	
annual mean temperature in °C	5.3	0.33 K/10 a, 99 % sign. winter: 0.52 K/10 a, 95 % sign.
annual temperature amplitude in K	18.1	
annual sum of precipitation in mm	1162.5	19 mm/10 a, not significant
month with maximum of precipitation	December, July	
snow cover **	approx. 80 days	−10 days/10 a, 95 % sign.

* Classification by Köppen/Trewartha/Rudloff according to Hendl (1991)
* Fichtelberg-Hüttstadl, 662 m a.s.l.

Table 2. Overview of the meteorological conditions at *Waldstein-Pflanzgarten* site during IOP-1 and IOP-2.

Parameter	IOP-1 (6 Sep to 7 Oct 2007)	IOP-2 (1 Jun to 15 Jul 2008)
mean temperature in °C	9.9 °C	15.2 °C
relation to normal	Sep too cold (t1.2 K); Oct too cold (t0.6 K)	Jun too warm (+1.5 K); Jul normal (+0.2 K)
absolute maximum temperature in °C	21.0 °C at 24 Sep 2007	28.9 °C at 22 Jun 2008
absolute minimum temperature in °C	2.8 °C at 19 Sep 2007	3.7 °C at 14 Jun 2008
precipitation sum in mm	113.2 mm	112.8 mm
relation to normal	Sep too wet, from 30 Sep no rain; Oct to dry.	Jun too dry, no rain from 18 Jun to 3 Jul except a thunderstorm at 25 Jun 2008; Jul normal
maximum daily sum precipitation in mm	22.1 mm at 27 Sep 2007	44.1 mm at 3 Jul 2008
mean incoming shortwave radiation in W m^{-2} (24 h)	80.4 W m^{-2}	225.6 W m^{-2}
maximum daily mean incoming shortwave radiation in W m^{-2}	152.5 W m^{-2} at 15 Sep 2007	342.7 W m^{-2} at 1 Jun 2008

Table 3. Overview of trace gas concentrations (ppb) and total of wet deposition (ionic components; mg m^{-2}) during the Intensive Observation Periods of the EGER project (IOP-1, IOP-2), measured at the *Waldstein-Weidenbrunnen* site (31 m a.gr.) and *Waldstein-Pflanzgarten* site (wet deposition, 1.5 m a.gr.), respectively.

Trace gas	IOP-1 6 Sep–3 Oct 2007	IOP-2 1 Jun–11 Jul 2008
ozone (O_3)	33 ppb (average) 50 ppb (95 % quantile)	55 ppb (average) 76 ppb (95 % quantile)
maximum O_3	59 ppb (23 Sep 2007)	85 ppb (6 Jun 2008)
nitric oxide (NO)	0.3 ppb (average) 1.1 ppb (95 % quantile)	0.2 ppb (average) 0.6 ppb (95 % quantile)
maximum NO	2.5 ppb at (2 Oct 2007	3.4 ppb (7 Jun 2008)
nitrogen dioxide (NO_2)	3.1 ppb (average) 6.7 ppb (95 % quantile)	2.5 ppb (average) 4.6 ppb (95 % quantile)
maximum NO_2	28.5 ppb (28 Sep 2007)	15.6 ppb (9 Jun 2008)
sulphur dioxide (SO_2)	N/A	0.8 ppb (mean) 2.6 ppb (95 % quantile)
maximum SO_2	N/A	10.8 ppb (9 Jun 2008)
total of wet deposition (ionic components)	IOP-1	IOP-2
Cl^-	55 mg m^{-2}	< 22 mg m^{-2}
NO_2^-	< 7 mg m^{-2}	< 4 mg m^{-2}
NO_3^-	297 mg m^{-2}	187 mg m^{-2}
SO_4^{2-}	199 mg m^{-2}	114 mg m^{-2}
NH_4^+	107 mg m^{-2}	78 mg m^{-2}
K^+	< 30 mg m^{-2}	< 18 mg m^{-2}
Mg^{2+}	5 mg m^{-2}	< 6 mg m^{-2}
Ca^{2+}	32 mg m^{-2}	36 mg m^{-2}

Table 4. Towers at the *Waldstein-Weidenbrunnen* site during the Intensive Observation Periods of the EGER project (IOP-1: 2007; IOP-2: 2008).

	Coordinates	Height [m]	Major equipment
"main tower"	50°08′31.2″ N 11°52′00.8″ E 775 m a.s.l.	31	FLUXNET station Wind-, dry and wet bulb temperature profiles Profiles of trace gas concentrations and fluxes Measurements of soil related quantities and trace gas soil flux measurements (dynamic chambers), within a radius of 10–50 m
"turbulence tower"	50°08′29.9″ N 11°52′03.1″ E	35	Profile of turbulent energy and carbon dioxide fluxes
"bio-tower"	50°08′32.9″ N 11°51′57.8″ E	36	Vertical profile of sapflow, temperature, humidity, and net radiation CO_2 and H_2O exchange measurements on spruce branches (dynamic cuvette)

Table 5. Remote sensing techniques used during the Intensive Observation Periods of the EGER project (IOP-1: 2007; IOP-2: 2008).

Device	Coordinates	Location
2-D sonic anemometer (Thies)	50°08′31.2″ N, 11°52′00.8″ E 775 m a.s.l. + 32 m	*Waldstein-Weidenbrunnen*, ,,main tower“
mini-sodar, SFAS (Scintec AG)	50°08′30.3″ N, 11°52′11.0″ E 785 m a.s.l.	clearing, NE of *Waldstein-Weidenbrunnen* site
Sodar/RASS, DSDPA90.64 (METEK GmbH)	50°08′35.3″ N, 11°51′48.8″ E 764 m a.s.l.	*Waldstein-Pflanzgarten*
UHF-windprofiler (Vaisala)	49.98° N, 11.68° E 514 m a.s.l.	*Oschenberg* near *Bayreuth*

Table 6. Turbulent flux measuring instrumentation at the *Waldstein-Weidenbrunnen* site during the Intensive Observation Periods of the EGER project (IOP-1: 2007; IOP-2: 2008).

	Height [m]	Sonic anemometer	Trace gas	Trace gas analyzer
“main tower” (IOP-1)	32	Solent R2, Gill Instruments Ltd.	CO_2, H_2O	LI-7500, L-COR Inc.
			O_3	GEFAS GmbH***
	1****	Solent R2, Gill Instruments Ltd.	O_3	GEFAS GmbH***
“main tower” (IOP-2)	32	USA-1, METEK GmbH	CO_2, H_2O	LI-7500, L-COR Inc.
	32	CSAT3, Campbell Sci. Inc.	NO, NO_2	CLD 790SR-2, Ecophysics
			O_3	NOAA/ATDD***
	25	Solent R2, Gill Instruments Ltd.	O_3	Enviscope GmbH***
	17	Solent R2, Gill Instruments Ltd.	O_3	Enviscope GmbH***
	1	Solent R2, Gill Instruments Ltd.	O_3	GEFAS GmbH***
“turbulence tower” (IOP-1, IOP-2)	36	USA-1, METEK GmbH	CO_2, H_2O	LI-7500, L-COR Inc.
	23	CSAT3, Campbell Sci. Inc.	CO_2, H_2O	LI-7500, L-COR Inc.
	18	Solent R3-50, Gill Instrum. Ltd.	CO_2, H_2O	LI-7500, L-COR Inc.
	13	CSAT3, Campbell Sci. Inc.	CO_2, H_2O	LI-7500, L-COR Inc.**
	5.5	CSAT3, Campbell Sci. Inc.*	CO_2, H_2O	LI-7500, L-COR Inc.
	2.5	CSAT3, Campbell Sci. Inc.	CO_2, H_2O	LI-7500, L-COR Inc.

* During IOP-1 Solent R2, Gill Instruments Ltd.;
** during IOP-1 KH20 Campbell Scientific, Inc.;
*** all fast-response O_3-analyzers were based on solid-phase chemiluminescence technique (Güsten and Heinrich, 1996), but designed by different manufacturers (indicated);
**** O_3-flux measurements at 1 m have been performed one week before those at 32 m (using the same instrumentation).

Table 7. Profile measurements at the "main tower" of the *Waldstein-Weidenbrunnen* site during the Intensive Observation Periods of the EGER project (IOP-1 and IOP-2).

	IOP-1 6 Sep–7 Oct 2007	IOP-2 1 Jun–15 Jul 2008
	measurement levels at "main tower" (in m)	
wind speed I	4.6, 10.0, 16.5, 18.0, 21.0, 25.0, 31.0	4.6, 10.0, 16.5, 18.0, 21.0, 25.0, 31.0
wind speed II	7.6, 13.3, 19.8, 24.3, 26.3, 31.3	7.6, 13.3, 19.8, 24.3, 26.3, 31.3
dry & wet bulb temperature I	5.0, 13.0, 21.0, 31.0	5.0, 13.0, 21.0, 31.0
(aspirated)	4.9, 9.9, 15.9, 19.5, 24.4, 26.6, 30.9	4.9, 9.9, 15.9, 19.5, 24.4, 26.6, 30.9
dry & wet bulb temperature II (aspirated)		
CO_2, H_2O, O_3, NO, NO_2	5.0, 10.0, 16.0, 24.2 (2x), 31.0	3.0, 10.0, 16.5 (2x), 20.5, 25.0, 31.5
NH_4NO_3, NH_3 and HNO_3	24.2, 30.4	N/A
HONO	24.5	N/A
NO, NO_2, O_3, CO_2 and H_2O exchange measurements on spruce branches (dynamic cuvette)	13.0	N/A
	measurement levels at "forest floor" (in m)	
wind speed I	2.0	2.0
wind speed II	0.04, 0.30, 1.0, 2.00	0.04, 0.3, 1.0, 2.0
dry & wet bulb temperature I	0.05, 2.0	0.05, 2.0
(aspirated)	0.09, 0.26, 1.00, 2.05	0.09, 0.26, 1.00, 2.05
dry & wet bulb temperature II (aspirated)	0.01, 0.02, 0.04, 0.08, 0.16, 0.32	0.01, 0.02, 0.04, 0.08, 0.16, 0.32
air temperature (non-aspirated)		
CO_2, H_2O, O_3, NO, NO_2	0.05, 0.3, 1.0, 2.0	0.005, 0.03, 0.1, 0.3, 0.9
$^{220}Rn/^{222}Rn$	0.04, 0.27	0.00, 0.03, 0.1, 0.3
HONO	0.5	1.0
	measurement levels at "bio-tower" (in m)	
air temperature & rel. humidity (aspirated)	9.3, 11.7, 14.8, 17.2, 20.2, 22.6	9.3, 11.7, 14.8, 17.2, 20.2, 22.6
net radiation	11.9, 17.4, 22.8	11.9, 17.4, 22.8
CO_2	N/A	0.03, 1.0, 16.0, 18.7, 21.4, 24.1, 29 ± 3, 36.0

Table A1. Coefficients for Eq. (A1).

Reference	i	a_i	α_i	β_i	γ_i
Rannik et al. (2003), neutral, for *Hyytiäla* site	u	2.30	1.0	1.0	−0.3
	v	1.75	1.0	0.85	−0.2
	w	1.25	0.9	1.2	−0.63
Waldstein-Weidenbrunnen site, IOP-1	u	2.01	8.97	1.37	0.29
	v	1.60	5.18	1.11	0.34
	w	1.13	0.9	1.2	−0.63

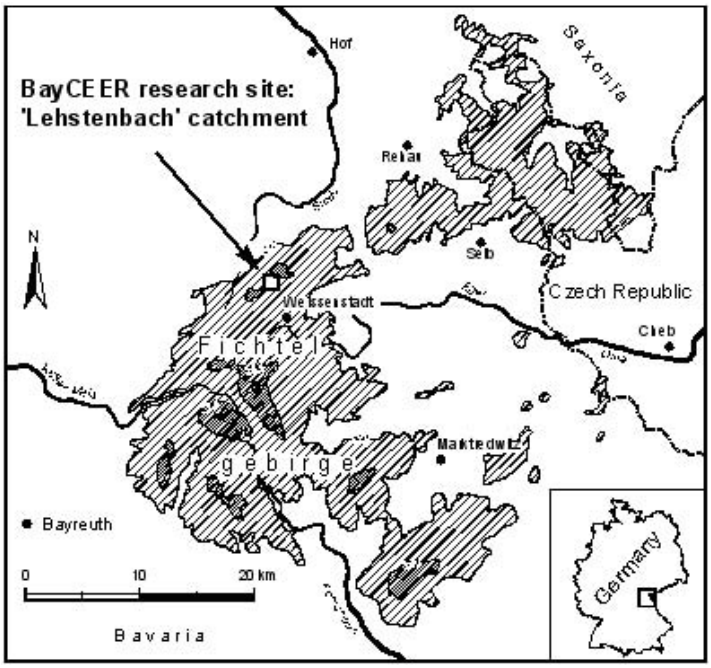

Fig. 1. Map of the "*Fichtelgebirge*" region (Gerstberger et al., 2004). The *Waldstein-Weidenbrunnen* site is located in the *Lehstenbach* catchment north-west of the small town *Weissenstadt* and the upper *Eger river* valley. Hatchings indicates elevations >500 m and >750 m a.s.l, respectively.

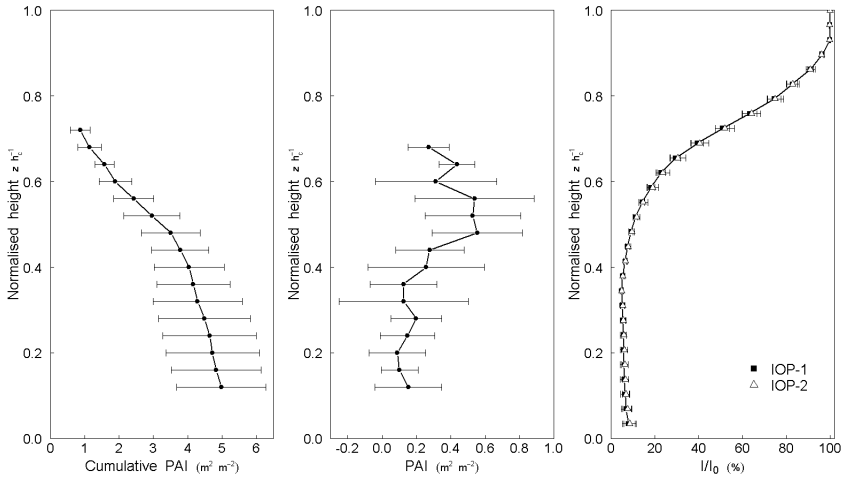

Fig. 2. Vertical profile of the (left) cumulative and (middle) absolute overstory plant area index (PAI) of the *Waldstein-Weidenbrunnen* site. Profiles are mean values of the five cumulative and absolute PAI profile measurements. Furthermore, the right figure shows the vertical distribution of the normalized shortwave radiation for both IOPs. The height is normalized by a canopy height of 25 m.

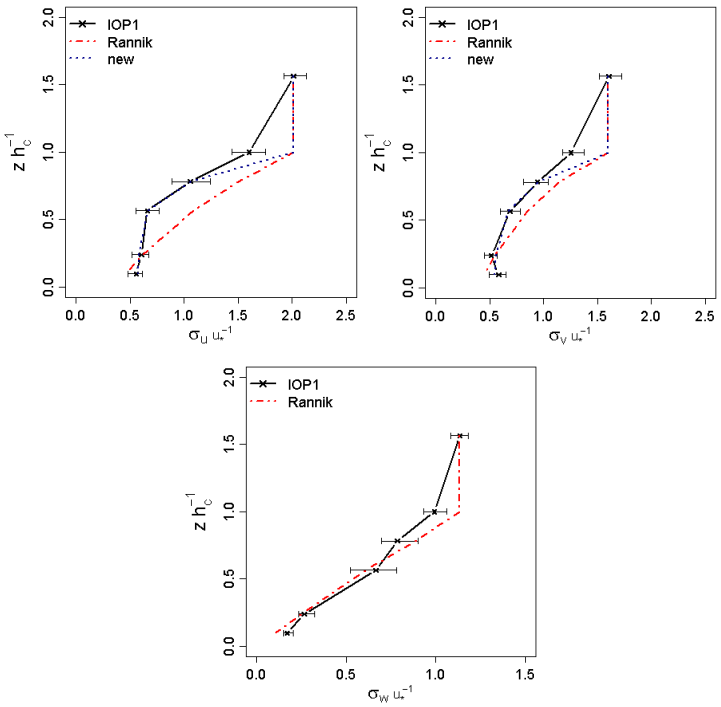

Fig. 3. Results of measurements (x, black line) and model parameterizations (red dot-dashed line) for profiles of the integral turbulence characteristics of wind velocity components u,v and w within the *Waldstein-Weidenbrunnen* forest stand and inside the lower roughness sublayer (near neutral stratification). For u and v the parameterization of Rannik et al. (2003) was modified to fit the measurements during IOP-1, for w the original coefficients were used, see Appendix.

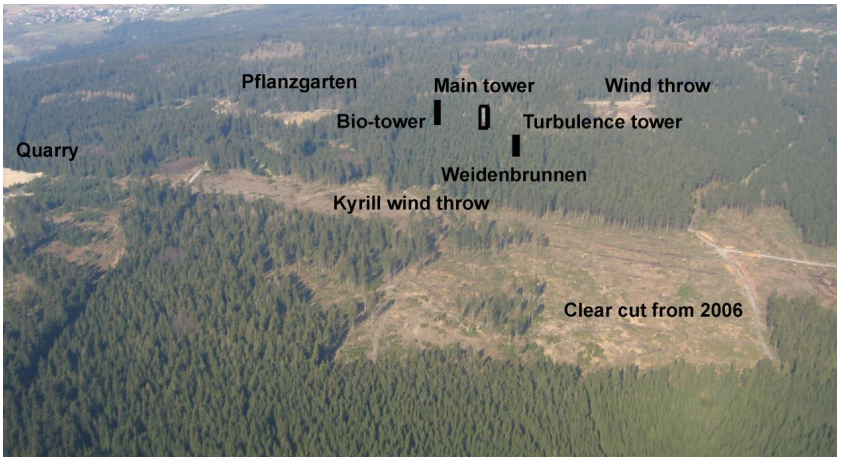

Fig. 4. The *Waldstein-Weidenbrunnen* site shortly after the "hurricane like" low pressure system "Kyrill" (view from south, photograph: Foken, T., 15 March 2007). The "main tower" can be seen within the *Waldstein-Weidenbrunnen* field site; "turbulence" and "bio" towers were set-up after 15 March 2007, but their locations are marked. The Modified Bowen-ratio system has been located at the wind throw north-east of the "turbulence tower".

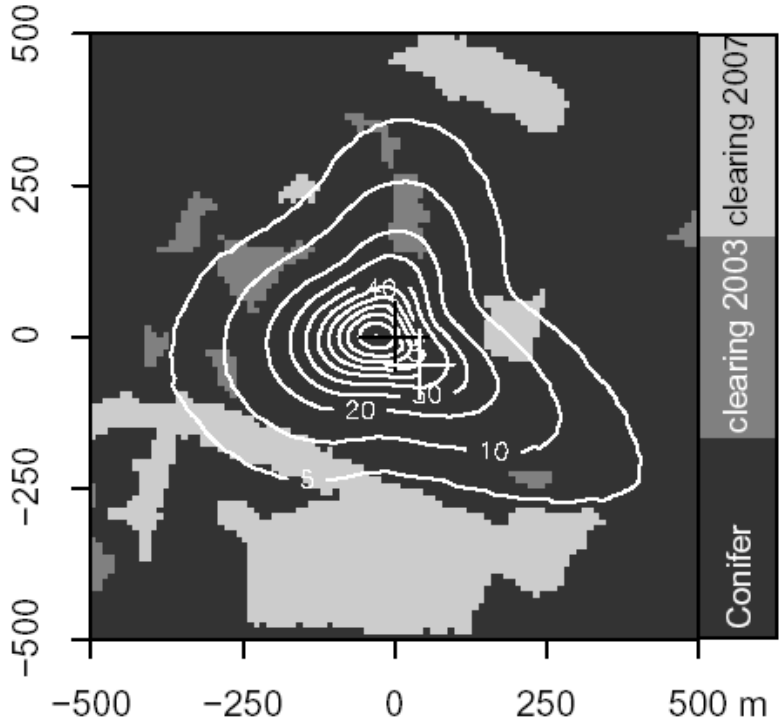

Fig. 5. Clear cuts in the planning phase of EGER (2003) and after "Kyrill" (18 January 2007). "Emma" on 1 March 2008 has affected the SW corner of the map. The black and white crosses indicate main and turbulence tower positions, respectively. White isolines indicate relative flux contribution to the footprint for 2003 data (Siebicke, 2008).

Fig. 6. Towers at the *Waldstein-Weidenbrunnen* site: **(a)** permanent main tower since 1996 (height 31 m) for routine measurements, FLUXNET station and chemical measurements, **(b)** turbulence tower (height 35 m) since 2007 with second FLUXNET complex and turbulence measurements, **(c)** biological tower (height 36 m) for gas exchange measurements at needles.

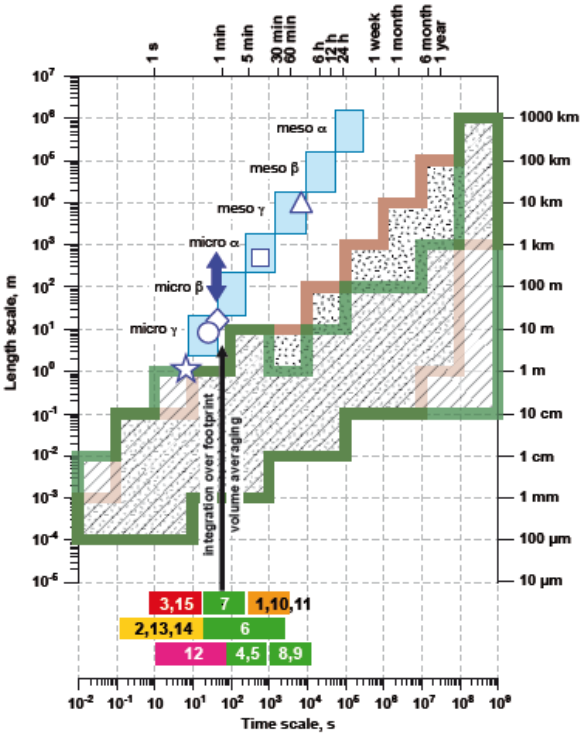

Fig. 7. Caption on next page.

Fig. 7. Temporal and spatial scales of atmospheric, turbulent, plant, physiological, soil and relevant chemical processes forming the conceptual backbone of the EGER project. Atmospheric Processes (Orlanski, 1975) are given in light blue squares of one order of magnitude (from *micro γ* to *meso α*). Forest canopy related transport processes comprise turbulent transport in canopy (white star), vertical advection in canopy (white circle), transport above canopy (white diamond), coherent structures (blue double arrow), footprint averaged turbulent flux (white square), and horizontal advection at canopy top (white triangle). The scales of plant processes, relevant for energy and matter exchange with the atmosphere (Schoonmaker, 1998), those of soil processes are shown by the brown framed, spotted area (Vogel and Roth, 2003; Blöschl and Sivapalan, 1995). Time scales of relevant chemical reactions are shown according to Dlugi (1993, updated): (1) $HO_2 + HO_2 \rightarrow H_2O_2 + O_2$, (2) $HNO_3 + NH_3 \leftrightarrow NH_4NO_3$, (3) $O_3 + NO \rightarrow NO_2 + O_2$, (4) O_3 + isoprene → reaction products (P), (5) O_3 + monoterpenes → P, (6) NO_3 + monoterpenes → P, (7) NO_3 + isoprene → P, (8) OH + isoprene → R, (9) OH + monoterpenes → R, (10) O_3 + olefins → R, (11) $O_3 + NO_2 \rightarrow NO_3 + O_2$, (12) $N_2O_5 + H_2O \rightarrow 2HNO_3$, (13) HNO_3 (+ H_2O) → $H^+ + NO_3^-$, (14) $H_2O + 2NO_2$ (het) → $HNO_2 + HNO_3$ (g), (15) $NO_2 + h\upsilon \rightarrow NO + O$ (for details of concentration ranges see Dlugi, 1993).

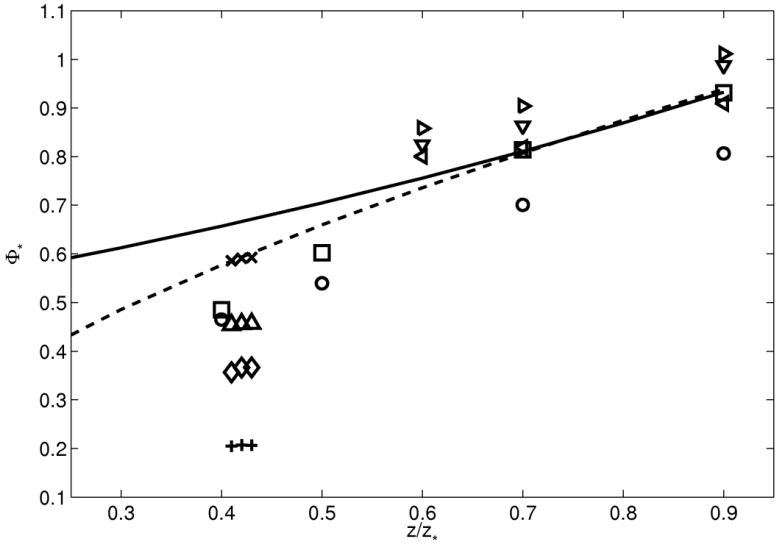

Fig. 8. The calculated ϕ_* values of the EGER data are presented by crosses, upward-pointing triangles, diamonds, and plus signs. The crosses represent u_* values smaller than 0.4 and larger than 0.2. Further the upward-pointing triangles represent $0.4 < u_* < 0.6$, the diamonds $0.6 < u_* < 0.8$ and the plus signs $0.8 < u_* < 1.2$. The calculated ϕ_* values of the COPS data for a canopy height of 1.2m are represented by squares and circles. The squares represent $0.2 < u_* < 0.3$ and the circles represent $0.3 < u_* < 0.6$. The calculated ϕ_* values of the COPS data for a canopy height of 2.9m are represented by downward-pointing, right-pointing, and left-pointing triangles. The downward-pointing triangles represent $0.2 < u_* < 0.3$, the right-pointing triangles display $0.3 < u_* < 0.4$ and left-pointing triangles $0.4 < u_* < 0.5$. Furthermore, the solid line represents the equation developed by Garratt (1992) and the dashed line represents the equation developed by Mölder et al. (1999).

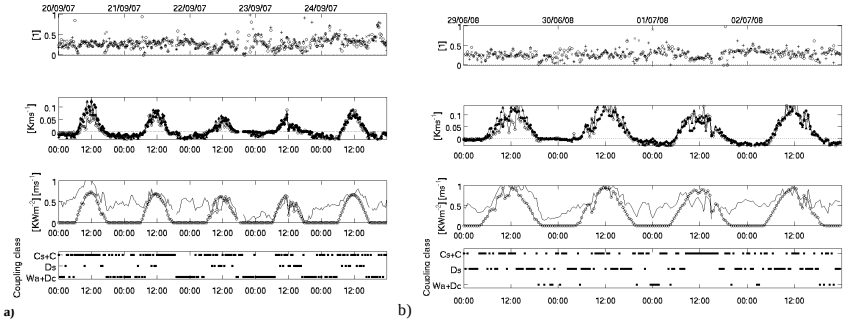

Fig. 9. Measurements and characterisation of the turbulent exchange for the period 20 to 24 September 2007 during IOP-1 **(a)** and 29 June to 2 July 2008 during IOP-2 **(b)**. Upper panel: relative flux contribution of coherent structures $F_{cs}F_{tot}^{-1}$ for carbon dioxide (open circles), buoyancy (crosses) and latent heat (pluses) at $1.44h_c$; second panel: kinematic buoyancy flux of coherent structures H_{cs} at $1.44h_c$ (filled circles), $0.93h_c$ (grey triangles) and $0.72h_c$ (open circles); third panel: friction velocity u_* (solid line), incoming shortwave radiation *Rg* (open circles) and wind direction (filled circles) at $1.44h_c$; lowest panel: coupling situations.

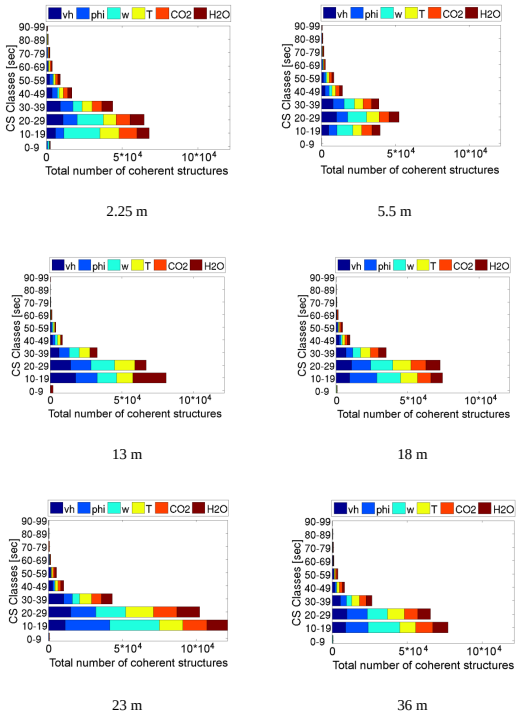

Fig. 10. Total number of coherent structures (CS) detected from 14 September 2007 until 08 October 2007 in carbon dioxide CO_2, water vapour H_2O, wind direction phi, sonic temperature T_s, horizontal wind velocity v_h, and vertical wind velocity w from measurements at the turbulence tower on six levels.

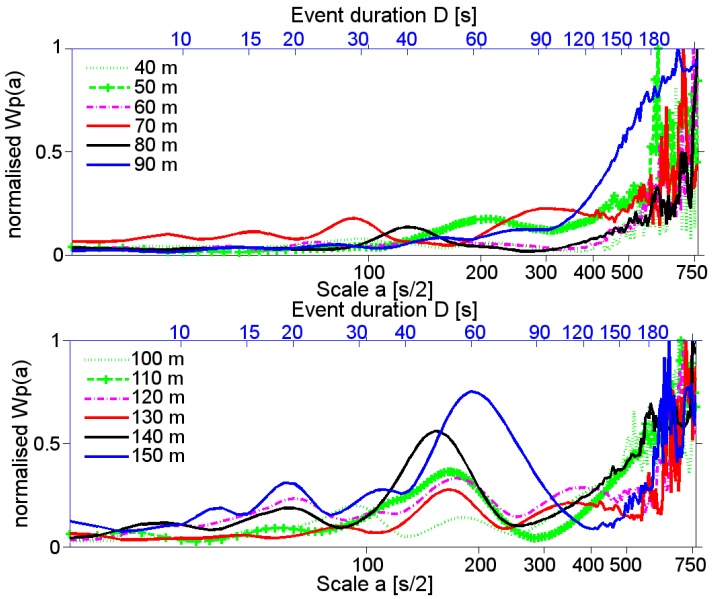

Fig. 11. Normalized spectra of the wavelet variance for different observation levels for the vertical wind during IOP-1 14 September 2007, 00:00–00:25 CET.

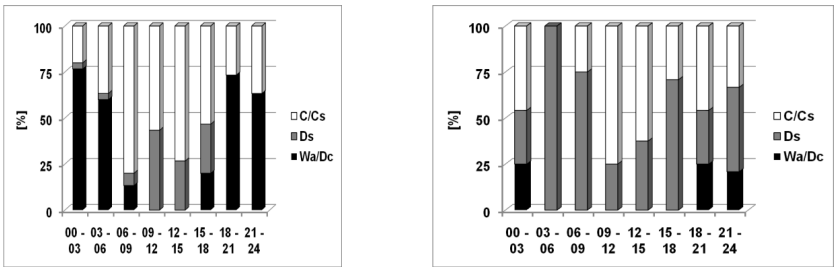

Fig. 12. Percentage of different coupling classes during the Golden Days of IOP-1(left, 30 three-hour periods) and IOP-2 (right, 24 three-hour periods) in the daily cycle.

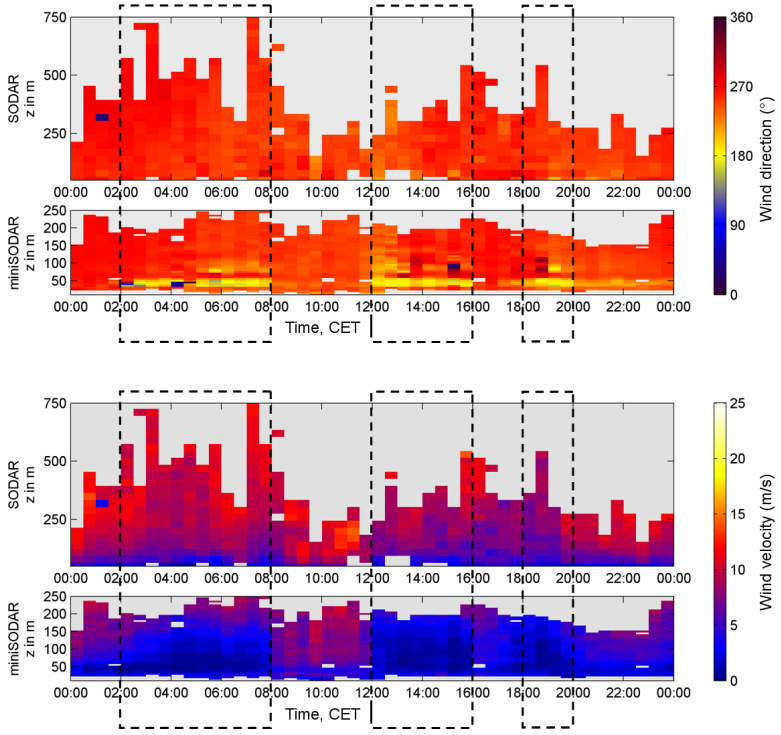

Fig. 13. Time-high profile from sodar and mini-sodar data of the wind direction (above) and the wind velocity (below) on 28 June 2008. Periods with southerly winds directly above the canopy originating from the clear-cut are highlighted.

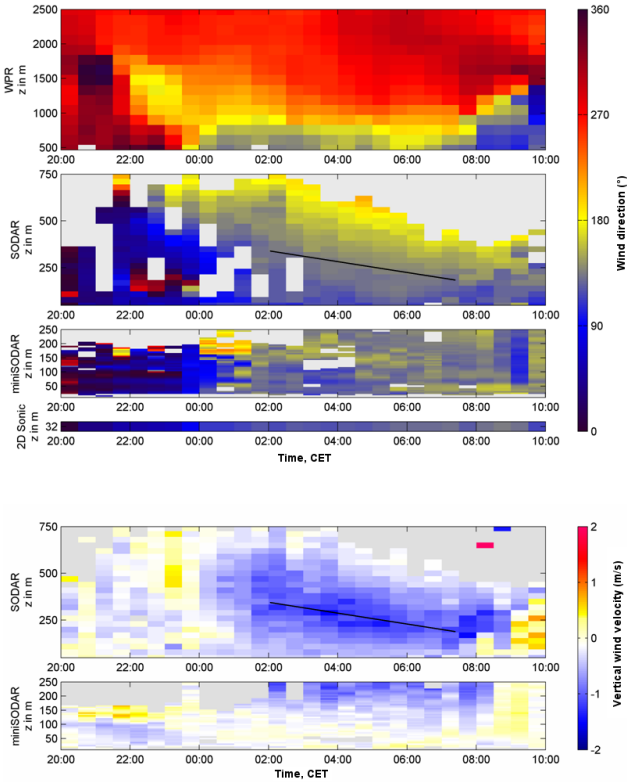

Fig. 14. Time-high profile from windprofiler, sodar, mini-sodar and sonic data of the horizontal wind velocity (above), the wind direction (middle), and vertical wind velocity (below) in the night from 30 June to 1 July 2008. The axis of the low-level jet is highlighted.

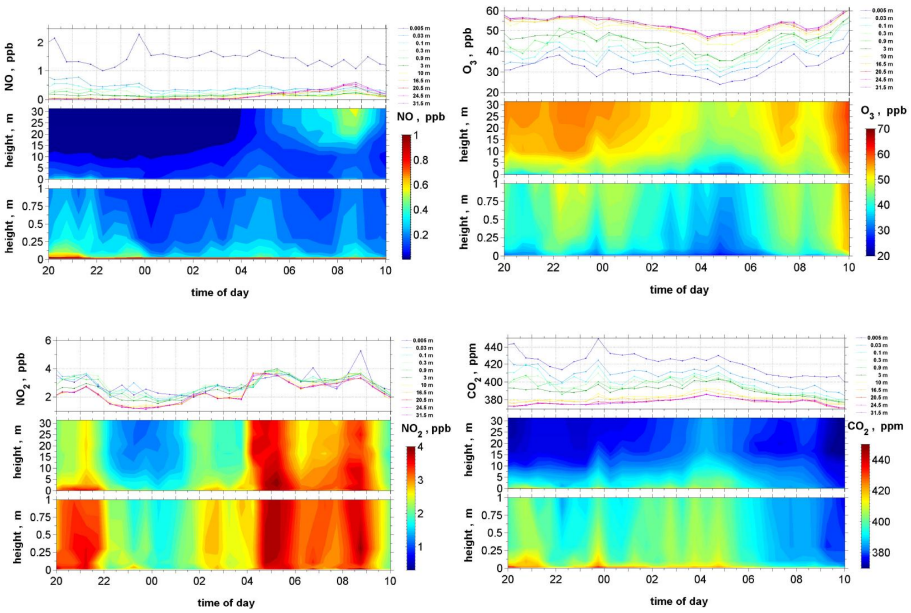

Fig. 15. Averaged vertical profiles in the night from 30 June to 1 July 2008 (compare with Fig. 14) for NO, NO_2, O_3 and CO_2 time in CET. For each trace gas the concentration at different levels, the concentration in and above the 25 m high forest and close to the forest floor are shown.

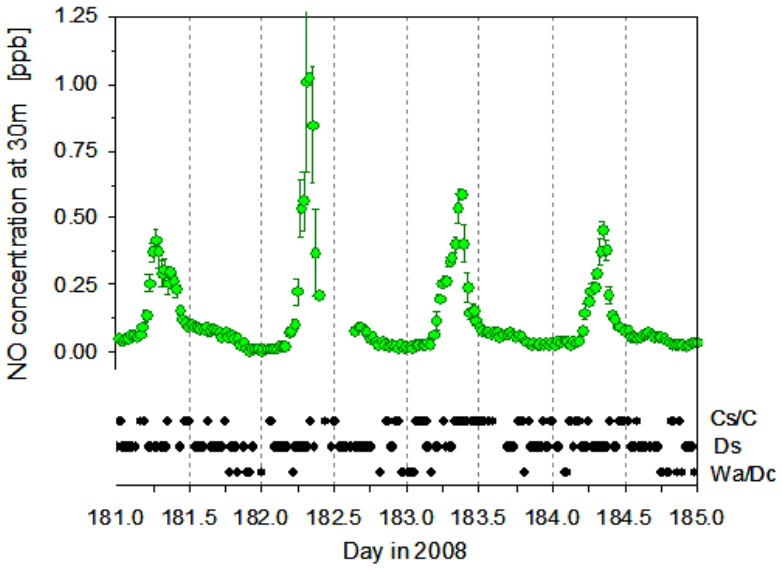

Fig. 16. Diel variation of NO concentration measured at *Waldstein-Weidenbrunnen* main tower (above canopy; 30 m a.gr.) from 29 June to 2 July 2008 (IOP-2). Original 5 Hz data have been averaged to 30 min means, error bars indicate corresponding standard deviations. Every day, between 06:00 and 12:00 (CET), when the convective boundary layer was still emerging, particularly high NO concentrations with large standard deviations were observed due to advection of freshly emitted exhaust gases from a busy (2100 cars day^{-1}) district road (HO18) running from SSE to NNW between 1 and 2 km distance west to the *Waldstein-Weidenbrunnen* site. The occurrence of canopy coupling stages (Cs/C, Ds, Wa/Dc) is given at the bottom.

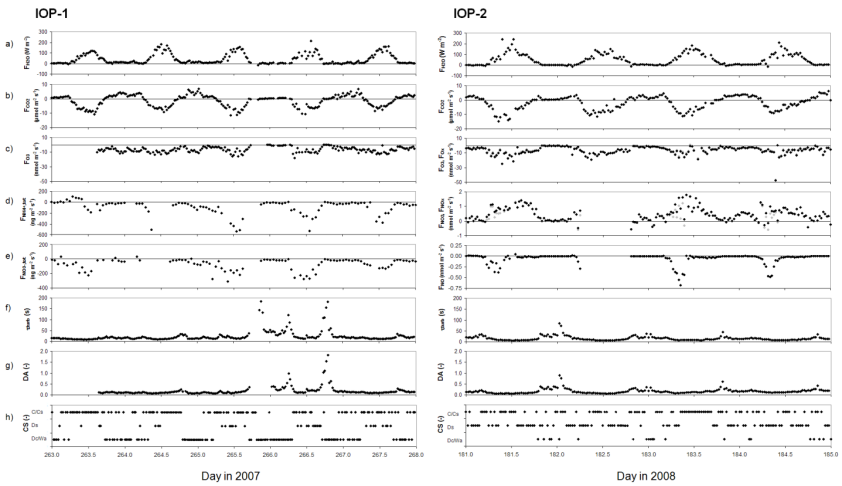

Fig. 17. Results of flux measurements of gaseous and particulate trace compounds at the "main tower" during 20–24 September 2007 (IOP-1, DOY 263–267, left panels) and for 29 June to 2 July 2008 (IOP-2, DOY 181–184, right panels). **(a)** F_{H_2O}, **(b)** F_{CO_2}, **(c)** F_{O_3} (black symbols) and F_{Ox} (grey symbols, IOP-2 only), **(d)** $F_{NH_4^+,tot}$ (left panel) and F_{NO_2} and F_{NO_x} (right panel, black and grey symbols, respectively), **(e)** $F_{NO_3^-,tot}$ (left panel) and F_{NO} (right panel), **(f)** turbulent time scale τ_{turb} (24–32 m), **(g)** Damköhler number *DA* (24–32 m), **(h)** coupling regimes (determined from measurements at the "turbulence tower", see Sect. 3.2). Measurement heights were 32 m (a. gr.) for all fluxes measured by eddy covariance during IOP-1 **(a–c)**, and during IOP-2 **(a–e)**; fluxes of total ammonium and total nitrate (**d** and **e**, IOP-1), determined by aerodynamic gradient technique, refer to 27.1 m (geometric mean of the heights of both intake levels).

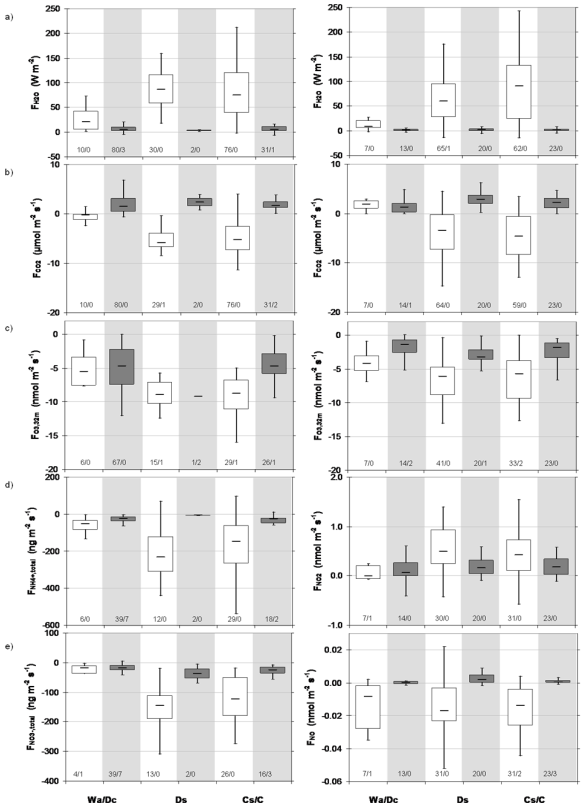

Fig. 18. Caption on next page.

Discussion Paper | Discussion Paper | Discussion Paper | Discussion Paper |

Fig. 18. Statistical dispersion and skewness of turbulent fluxes (F) of gaseous and particulate trace compounds at the "main tower" for 20–24 September 2007 (IOP-1, DOY 263–267, left panels) and for 29 June to 2 July 2008 (IOP-2, DOY 181–184, right panels): F_{H_2O} **(a)**, F_{CO_2} **(b)**, F_{O_3} **(c)**, $F_{NH_4^+,tot}$ (**d**, left panel), F_{NO_2} (**d**, right panel), $F_{NO_3^-,tot}$ (**e** left panel), and F_{NO} (**e** right panel). Data were classified by coupling regimes (Wa/Dc, decoupled conditions; Ds, decoupled subcanopy; Cs/C, coupled subcanopy by sweeps and fully coupled subcanopy) and day- (open box-plots) and night-time (grey shades). Remark: the bottom and top of each box represent the 25th and 75th percentile, the horizontal bar within each box is the 50th percentile (median); horizontal bars at the end of the whiskers stand for the lowest (highest) value still within 1.5 times the inter-quartile range of the lower (upper) quartile. Values exceeding those whisker ends (minimum and maximum outliers) are not depicted in the graphs, yet their number m (of the total number n) is indicated at the bottom of each box as "n/m".

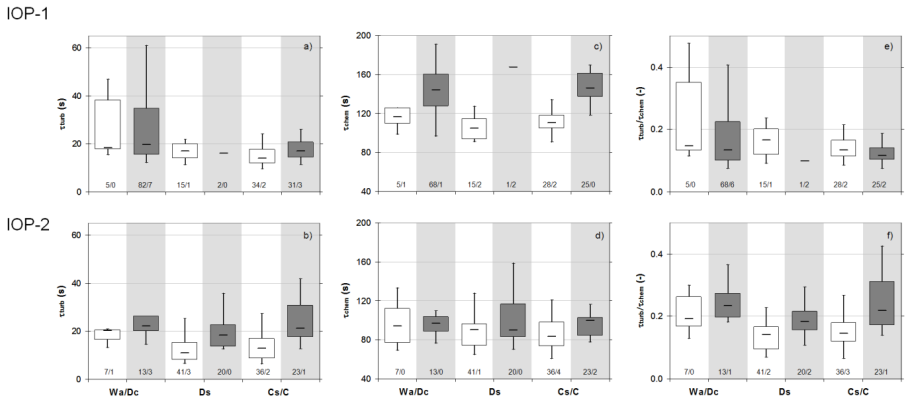

Fig. 19. Statistical dispersion and skewness of turbulent time scale τ_{turb} **(a, b)**, chemical time scale τ_{chem} **(c, d)**, and Damköhler number *DA* (= τ_{turb} / $\tau_{chem.}$; **e, f)** at the "main tower" for 20–24 September 2007 (IOP-1, DOY 263–267, top panels), and for 29 June to 2 July 2008 (IOP-2, DOY 181–184, bottom panels), classified by coupling regimes (Wa/Dc, decoupled conditions; Ds, decoupled subcanopy; Cs/C, coupled subcanopy by sweeps and fully coupled subcanopy) and day- (open box-plots) and night-time (grey shades). See remark on Fig. 18.

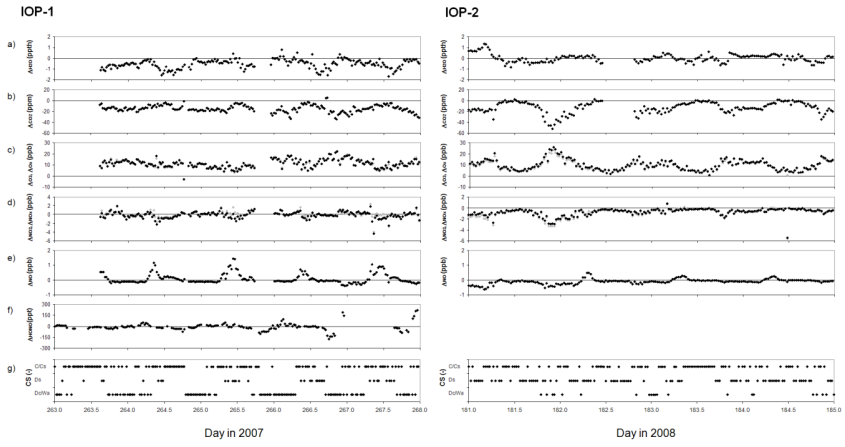

Fig. 20. Concentration differences $\Delta[C] = [C]_{24m} - [C]_{0.9m}$ between the 24 m and the 0.9 m level at the "main tower" for 20–24 September 2007 (IOP-1, DOY 263–267, left panels), and for 29 June to 2 July 2008 (IOP-2, DOY 181–184, right panels): **(a)** $\Delta[H_2O]$, **(b)** $\Delta[CO_2]$, **(c)** $\Delta[O_3]$ and $\Delta[O_x]$ (black and grey symbols, respectively), **(d)** $\Delta[NO_2]$ and $\Delta[NO_x]$ (black and grey symbols, respectively), **(e)** Δ[NO], **(f)** Δ[HONO] (IOP-1 only); **(g)** coupling regimes (determined from measurements at the "turbulence tower", see Sect. 3.2).

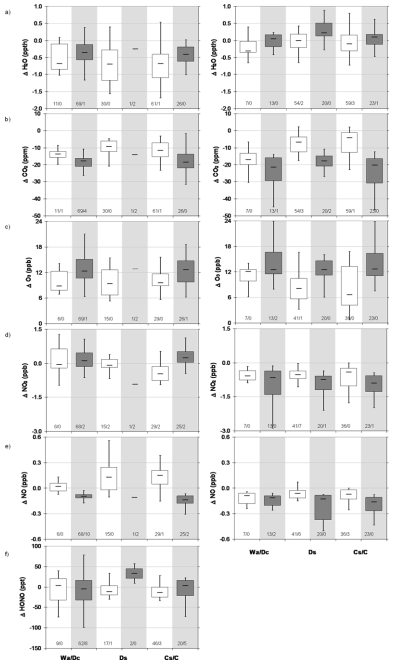

Fig. 21. Statistical dispersion and skewness of concentration differences Δ at the "main tower" for 20–24 September 2007 (IOP-1, DOY 263–267, left panels) and for 29 June to 2 July 2008 (IOP-2, DOY 181–184, right panels): ΔH_2O **(a)**, ΔCO_2 **(b)**, ΔO_3 **(c)**, ΔNO_2 **(d)**, ΔNO **(e)**, and ΔHONO (f, IOP-1 only). Data were classified by coupling regimes (Wa/Dc, decoupled conditions; Ds, decoupled subcanopy; Cs/C, coupled subcanopy by sweeps and fully coupled subcanopy) and day- (open box-plots) and night-time (grey shades). See remark on Fig. 18.

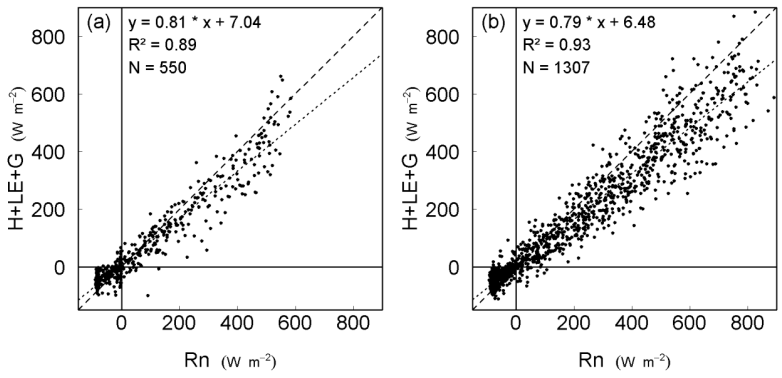

Fig. 22. Energy balance closure at the turbulence tower during IOP-1 (left) and IOP-2 (right).

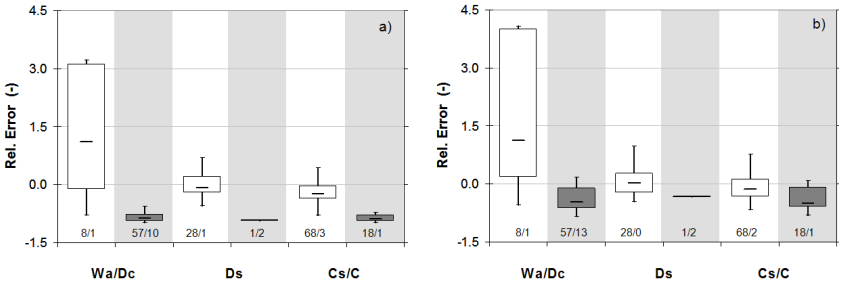

Fig. 23. Statistical dispersion and skewness of relative model error with respect to coupling stages (for definition see text) from **(a)** STANDFLUX, and **(b)** ACASA; measured and modelled evapotranspiration data ranged from 20 September through 24 September 2007 (IOP-1, DOY 263–267); measured evapotranspiration from turbulence tower 36 m level. Data were classified by coupling regimes (Wa/Dc, decoupled conditions; Ds, decoupled subcanopy; Cs/C, coupled subcanopy by sweeps and fully coupled subcanopy) and day- (open box-plots) and night-time (grey shades). See remark on Fig. 18.